PHYSICAL REVIEW C **89**, 065211 (2014)

The reaction $\pi N \to \pi\pi N$ in chiral effective field theory with explicit $\Delta(1232)$ degrees of freedom

D. Siemens[*]
Institut für Theoretische Physik II, Ruhr-Universität Bochum, D-44780 Bochum, Germany

V. Bernard[†]
Institut de Physique Nucléaire, CNRS/Université Paris-Sud 11 (UMR 8608), F-91406 Orsay Cedex, France

E. Epelbaum[‡] and H. Krebs[§]
Institut für Theoretische Physik II, Ruhr-Universität Bochum, D-44780 Bochum, Germany

Ulf-G. Meißner[‖]
Helmholtz-Institut für Strahlen- und Kernphysik and Bethe Center for Theoretical Physics, Universität Bonn, D-53115 Bonn, Germany and Institute for Advanced Simulation, Institut für Kernphysik, Jülich Center for Hadron Physics, and JARA—High Performance Computing Forschungszentrum Jülich, D-52425 Jülich, Germany

(Received 31 March 2014; published 30 June 2014)

The reaction $\pi N \to \pi\pi N$ is studied at tree level up to next-to-leading order in the framework of manifestly covariant baryon chiral perturbation theory with explicit $\Delta(1232)$ degrees of freedom. Using total cross-section data to determine the relevant low-energy constants, predictions are made for various differential as well as total cross sections at higher energies. A detailed comparison of results based on the heavy-baryon and relativistic formulations of chiral perturbation theory with and without explicit Δ degrees of freedom is given.

DOI: 10.1103/PhysRevC.89.065211 PACS number(s): 25.80.Hp, 12.39.Fe, 11.30.Rd, 14.20.Gk

I. INTRODUCTION

Chiral perturbation theory (χPT) is nowadays a standard tool to analyze low-energy hadronic reactions in harmony with the symmetries of QCD. It was originally formulated by Weinberg [1] and, a few years later, extended and applied by Gasser and Leutwyler to study the low-energy dynamics of the Goldstone bosons at the one-loop level in both the SU(2) [2] and the SU(3) [3] sectors. Starting with the pioneering work by Gasser *et al.* [4], χPT has also been extensively used in the baryon sector (see Refs. [5–7] for review articles, and references therein). In the framework of χPT, low-energy hadronic observables are calculated within the chiral expansion, where the expansion parameter Q is defined as the ratio of the soft scales corresponding to external momenta, denoted generically by q, or the pion mass M_π, and the chiral symmetry breaking scale $\Lambda_\chi \sim 1$ GeV. While in the Goldstone boson sector the hard scale Λ_χ only enters the amplitude through values of the low-energy constants (LECs) so that pion loop integrals calculated using dimensional regularization automatically fulfill the chiral power counting, special treatment of the nucleon mass $m_N \sim \Lambda_\chi$ is required in the baryon sector. The standard way to maintain the power counting in the nucleon sector is to use the heavy-baryon (HB) version of the effective Lagrangian [8,9]. In the heavy-baryon formulation of chiral perturbation theory (HBχPT), the nucleon mass does not appear in the propagators and enters only in the form of $1/m_N$ corrections to the vertices, which leads to the same suppression of dimensional regularization loop integrals as in the Goldstone boson sector. It is, however, known that the HB expansion has, for certain observables such as some of the nucleon electroweak and scalar form factors [10,11], a very limited range of convergence. It is thus advantageous to use a manifestly Lorentz-invariant effective Lagrangian rather than its HB version. Power counting can still be maintained using the method of Becher and Leutwyler [11] to extract the soft (i.e., infrared singular) parts of the loop integrals leading to the so-called infrared regularized χPT. Alternatively, the proper chiral scaling of the loop integrals can be restored in the covariant framework by imposing the appropriate renormalization conditions as proposed in Refs. [12,13] within the so-called extended on-mass-shell scheme. We refer the reader to Ref. [7] for a detailed discussion and comparison of the various χPT formulations and their applications in the single-baryon sector; see also Ref. [14] for a recent application of these ideas in the two-nucleon sector.

Another popular idea for extending the range of applicability of χPT in the nucleon sector is based on the explicit treatment of the $\Delta(1232)$, the close-by resonance with an excitation energy of $\Delta \equiv m_\Delta - m_N = 293$ MeV. All effects of the Δ in the standard approach are encoded in the LECs of pion-nucleon interactions beyond leading order (LO). The low excitation energy of the Δ and its strong coupling to the πN system lead, however, to unnaturally large values of certain LECs, which can, potentially, spoil the convergence of the chiral expansion. One can, therefore, argue that the *explicit* inclusion of the Δ in χPT by treating the Δ-nucleon mass splitting as a soft scale will allow us to resum a certain class of important contributions and improve the convergence compared to the Δ-less theory [15,16]. The

[*]dmitrij.siemens@rub.de
[†]bernard@ipno.in2p3.fr
[‡]evgeny.epelbaum@rub.de
[§]hermann.krebs@rub.de
[‖]meissner@hiskp.uni-bonn.de

improved convergence of HBχPT-Δ compared to the standard HBχPT has indeed been confirmed for πN scattering [17], proton Compton scattering (see [18] and references therein), nuclear forces (see, e.g., [19–21]), and other processes (see Ref. [7] for a review). It should, however, be emphasized that the explicit inclusion of the Δ makes calculations in the covariant framework considerably more involved and also leads to the appearance of additional LECs.

In the present work we analyze in detail single-pion production off nucleons from threshold up to the Δ resonance region using various formulations of χPT. The reaction $\pi N \to \pi\pi N$ has already attracted considerable interest on the experimental and theoretical sides which, historically, goes back to the possibility of using this process for the extraction of the $\pi\pi$ scattering lengths (see Refs. [22–24] in the context of χPT and a more general discussion in Ref. [25] with references to earlier work). Single-pion production off nucleons is also of special interest from the point of view of χPT. First of all, it involves three pions in the initial and final states so that one may expect for the scattering amplitude to be strongly constrained by the chiral symmetry of QCD. It therefore provides an excellent testing ground for χPT. On the other hand, the relatively high energies involved in this pion production reaction and the proximity of resonances with a strong coupling to the $\pi\pi N$ final state make the pursuit of a theoretical description of this reaction rather challenging. One expects for this process to be particularly well suited for studying the role of the Δ isobar, relativistic effects and unitarity and thus for testing various available formulations of χPT. Indeed, in Ref. [26] a relativistic tree level calculation including the Δ and the Roper resonance with LO pion-baryon vertices (i.e. dimension one couplings only) was performed and the appearing parameters were determined from other sources. The resulting total and differential cross section data were generally well described, encouraging further studies in baryon χPT. Last but not least, it is worth mentioning that the reaction $\pi N \to \pi\pi N$ provides complementary information to pion-nucleon scattering in the sense that it is sensitive to certain LECs which cannot be extracted from the πN system. The most prominent example is the LEC d_{16} which governs the quark mass dependence of the nucleon axial vector coupling constant. As a matter of fact, the lack of knowledge of its precise value represents one of the main sources of theoretical uncertainty in chiral extrapolations of nuclear observables [27–33].

All these arguments provide a strong motivation to take a fresh look at the reaction $\pi N \to \pi\pi N$ in the framework of χPT. In Refs. [24,34], it was analyzed within HBχPT at tree- and leading one-loop levels, respectively. A tree-level calculation based on the relativistic pion-nucleon Lagrangian is reported in Ref. [35]. The role of unitarity corrections in a HB calculation was in particular stressed in Ref. [36]. While these studies already showed that the predictions of χPT are in a satisfactory agreement with experimental data, we expect to be able to improve on them in the Δ region by explicitly taking into account the Δ degrees of freedom systematically, extending the earlier work of Ref. [26]. To the best of our knowledge, no calculations of this reaction using χPT with explicit Δ's beyond the LO pion-baryon couplings has been performed. In this paper we fill this gap and study single-pion production off nucleons in the framework of relativistic baryon χPT with explicit Δ degrees of freedom at *complete* tree level with the inclusion of the terms from the dimension-two effective Lagrangian.

Our paper is organized as follows. In Sec. II we discuss the relevant terms in the effective pion-nucleon-Δ Lagrangian. The decomposition of the transition matrix elements into the corresponding invariant amplitudes is considered in Sec. III while the relevant observables are defined in Sec. V. Section IV specifies all tree-level contributions to the amplitude up to next-to-leading order (NLO). The details of the calculation and the fitting procedure are reported in Sec. VI, while predictions for observables not used in the fitting procedure are collected in Sec. VII. Finally, the main results of our study are summarized in Sec. VIII. The Appendix contains explicit expressions for the kinematical variables and weight functions we use.

II. EFFECTIVE LAGRANGIAN

We employ the so-called small-scale expansion or ε expansion throughout this work, with the expansion parameter being defined as [16]

$$\varepsilon \in \left\{ \frac{q}{\Lambda_\chi}, \frac{M_\pi}{\Lambda_\chi}, \frac{\Delta}{\Lambda_\chi} \right\}; \tag{1}$$

i.e., the Δ-nucleon mass splitting is treated on the same footing as the pion mass (see, however, Ref. [37] for an alternative power counting scheme). We now discuss the terms in the effective Lagrangian relevant for our calculation.

The relativistic effective Lagrangian needed to describe pion-nucleon dynamics at tree level consists of the following pieces (see Ref. [38] for a full list of terms),

$$\mathcal{L}_{\rm eff} = \mathcal{L}^{(2)}_{\pi\pi} + \mathcal{L}^{(1)}_{\pi N} + \mathcal{L}^{(2)}_{\pi N} + \mathcal{L}^{(1)}_{\pi\Delta} + \mathcal{L}^{(2)}_{\pi\Delta} + \mathcal{L}^{(1)}_{\pi N\Delta} + \mathcal{L}^{(2)}_{\pi N\Delta}, \tag{2}$$

where the superscripts refer to the chiral dimension. The first term in Eq. (2) describes the meson interaction,

$$\mathcal{L}^{(2)}_{\pi\pi} = \frac{F_\pi^2}{4} \langle \partial_\mu U^\dagger \partial^\mu U \rangle + \frac{F_\pi^2 B}{2} \langle \mathcal{M} U^\dagger + U \mathcal{M} \rangle , \tag{3}$$

where the pions are collected in the SU(2) matrix-valued field $U(x) = u(x)^2$ given by

$$U = 1 + \mathrm{i}\frac{\boldsymbol{\tau}\cdot\boldsymbol{\pi}}{F_\pi} - \frac{\boldsymbol{\pi}^2}{2F_\pi^2} - \mathrm{i}\alpha\frac{\boldsymbol{\pi}^2\boldsymbol{\tau}\cdot\boldsymbol{\pi}}{F_\pi^3} + \frac{(8\alpha-1)}{8F_\pi^4}\boldsymbol{\pi}^4 + \cdots , \tag{4}$$

where α is a constant representing the freedom in the definition of the pion field. Further, F_π is the pion decay constant,[1] $\mathcal{M} = \mathrm{diag}(m_u, m_d)$ is the quark mass matrix, and B is an LEC.

[1]Since the calculation in the present work is carried out at the tree level, we do not have to differentiate between the pion decay constant in the chiral limit and its physical value. The same applies also to other quantities such as the nucleon mass and the nucleon axial vector coupling.

The next two terms in Eq. (2) give the leading and subleading pion-nucleon Lagrangians,

$$\begin{aligned}\mathcal{L}^{(1)}_{\pi N} &= \bar\Psi\left[\mathrm{i}\not{D} - m_N + \frac{g_A}{2}\not{u}\gamma_5\right]\Psi,\\ \mathcal{L}^{(2)}_{\pi N} &= \bar\Psi\left[c_1\langle\chi_+\rangle + c_2\left(-\frac{1}{8m_N^2}\langle u_\mu u_\nu\rangle\{D^\mu,D^\nu\} + \text{H.c.}\right)\right.\\ &\quad + \frac{c_3}{2}\langle u\cdot u\rangle - \frac{c_4}{8}[\gamma^\mu,\gamma^\nu][u_\mu,u_\nu]\\ &\quad \left. + c_5\left(\chi_+ - \frac{\langle\chi_+\rangle}{2}\right)\right]\Psi,\end{aligned} \tag{5}$$

where m_N and g_A denote the nucleon mass and axial vector coupling, c_i's refer to further LECs, and the proton and neutron are given in the isodoublet representation,

$$\Psi = \begin{pmatrix} p \\ n \end{pmatrix}. \tag{6}$$

The covariant derivative in Eq. (5) in the absence of external sources is defined via

$$D_\mu = \partial_\mu + \Gamma_\mu \quad \text{with} \quad \Gamma_\mu = \tfrac{1}{2}(u^\dagger\partial_\mu u + u\,\partial_\mu u^\dagger). \tag{7}$$

In addition, the abbreviation

$$\chi_+ = u^\dagger\chi u^\dagger + u\chi^\dagger u \quad \text{with} \quad \chi = 2B_0\mathcal{M} \tag{8}$$

and the chiral vielbein

$$u_\mu = \mathrm{i}(u^\dagger\partial_\mu u - u\,\partial_\mu u^\dagger) \tag{9}$$

are used.

The inclusion of the $\Delta(1232)$ as an explicit degree of freedom adds the last four terms to the effective Lagrangian in Eq. (2). The Δ isobar is described by a Rarita-Schwinger isospurion Ψ^i_μ, a spin-3/2 field, which is constructed via coupling of a spin-1 to a spin-1/2 field, treated as an isodoublet with an additional isovector index $i \in \{1,2,3\}$. The pion-Δ Lagrangian up to second order reads [16,17]

$$\begin{aligned}\mathcal{L}^{(1)}_{\pi\Delta} &= -\bar\Psi^\mu_i\left[(\mathrm{i}\not{D}^{ij} - m_\Delta\delta^{ij})g_{\mu\nu} - \mathrm{i}\left(\gamma_\mu D^{ij}_\nu + \gamma_\nu D^{ij}_\nu\right)\right.\\ &\quad + \mathrm{i}\gamma_\mu\not{D}^{ij}\gamma_\nu + m_\Delta\delta^{ij}\gamma_\mu\gamma_\nu + \frac{g_1}{2}g_{\mu\nu}\not{u}^{ij}\gamma_5\\ &\quad \left. + \frac{g_2}{2}\left(\gamma_\mu u^{ij}_\nu + u^{ij}_\mu\gamma_\nu\right)\gamma_5 + \frac{g_3}{2}\gamma_\mu\not{u}^{ij}\gamma_5\gamma_\nu\right]\Psi^\nu_j,\\ \mathcal{L}^{(2)}_{\pi\Delta} &= \frac{c_1^\Delta}{2}\bar\Psi^i_\mu\Theta^{\mu\alpha}(z)\gamma_{\alpha\beta}\delta^{ij}\,\langle\chi_+\rangle\,\Theta^{\beta\nu}(z)\Psi^j_\nu + \text{H.c.} + \cdots,\end{aligned} \tag{10}$$

where terms with two or more pion fields in $\mathcal{L}^{(2)}_{\pi\Delta}$ are not shown since they do not contribute to the reaction $\pi N \to \pi\pi N$ at order ε^2. Here, the quantity $\Theta^{\mu\alpha}(z)$ is defined via $\Theta^{\mu\alpha}(z) = g^{\mu\alpha} + z\gamma^\mu\gamma^\alpha$, and z, g_2, and g_3 denote the so-called off-shell parameters. Note that the dependence of the amplitude on such off-shell parameters can be absorbed into a redefinition of the corresponding LECs (see Refs. [39–41] for more details). It is, therefore, convenient to choose

$$z = g_2 = g_3 = 0, \tag{11}$$

which specifies our conventions for the calculations in the manifestly covariant framework. Here and in what follows, we show explicitly the dependence on some of the off-shell parameters in order to maintain consistency between the covariant and the HB calculations, as explained below. The covariant derivative in Eq. (10) is given by

$$D^{ij}_\mu = \partial_\mu\delta^{ij} + \Gamma^{ij}_\mu \quad \text{with} \quad \Gamma^{ij}_\mu = \Gamma_\mu\delta^{ij} - \mathrm{i}\epsilon^{ijk}\,\langle\tau^k\Gamma_\mu\rangle\,. \tag{12}$$

Finally, the pion-nucleon-Δ Lagrangian reads [16,17]

$$\begin{aligned}\mathcal{L}^{(1)}_{\pi N\Delta} &= h_A\left[\bar\Psi^i_\mu\Theta^{\mu\alpha}(z)w^i_\alpha\Psi_N + \bar\Psi w^i_\alpha\Theta^{\alpha\mu}(z)\Psi^i_\mu\right],\\ \mathcal{L}^{(2)}_{\pi N\Delta} &= \bar\Psi^i_\mu\Theta^{\mu\alpha}(z)\left[\mathrm{i}b_3 w^i_{\alpha\beta}\gamma^\beta + \frac{b_4}{2}w^i_\alpha w^j_\beta\gamma^\beta\gamma_5\tau^j\right.\\ &\quad \left. + \frac{b_5}{2}w^j_\alpha w^i_\beta\gamma^\beta\gamma_5\tau^j + \frac{b_6}{m_N}\mathrm{i}w^i_{\alpha\beta}\mathrm{i}D^\beta\right]\Psi + \text{H.c.},\end{aligned} \tag{13}$$

where h_A is the $\pi N\Delta$ axial coupling, b_i are further LECs, and

$$w^i_\alpha = \tfrac{1}{2}\mathrm{Tr}[\tau^i u_\alpha] \quad \text{and} \quad w^i_{\alpha\beta} = \tfrac{1}{2}\mathrm{Tr}[\tau^i[D_\alpha,u_\beta]]. \tag{14}$$

It should be emphasized that the free spin-3/2 Lagrangian is nonunique and usually written in terms of an unphysical "gauge" parameter A, whose entire dependence of the observables can be absorbed into redefinition of the Δ field. We have not shown explicitly the dependence on the parameter A in the effective Lagrangian by making the choice $A = -1$. This particular choice is convenient in the covariant approach since it leads to the simplest form of the free Lagrangian and thus also of the free Δ propagator,

$$\begin{aligned}\mathcal{G}^{\mu\nu}_\Delta(p) = -\frac{\not{p} + m_\Delta}{p^2 - m_\Delta^2}\left(g^{\mu\nu} - \frac{1}{3}\gamma^\mu\gamma^\nu\right.\\ \left. + \frac{1}{3}\frac{p^\mu\gamma^\nu - p^\nu\gamma^\mu}{m_\Delta} - \frac{2}{3}\frac{p^\mu p^\nu}{m_\Delta^2}\right).\end{aligned} \tag{15}$$

Since we are particularly interested here in the role of relativistic effects, we also carry out the calculations within HBχPT. In this approach, the nucleon four-momentum p_μ is separated into a large piece close to the on-shell kinematics and a soft residual contribution k_μ via

$$p_\mu = m_N\,v_\mu + k_\mu, \tag{16}$$

with v_μ being the four-velocity of the nucleon with the properties $v^2 = 1$ and $v^0 \geqslant 1$. The nucleon field Ψ is decomposed into eigenstates of $\not{v}$ with eigenvalues $+1$ and -1, the so-called "light" and "heavy" fields, respectively,

$$\begin{aligned}N_v &= e^{\mathrm{i}m_N v\cdot x}P^+_v\Psi,\\ h_v &= e^{\mathrm{i}m_N v\cdot x}P^-_v\Psi,\end{aligned} \tag{17}$$

with the projection operators $P^\pm_v = \frac{1}{2}(1 \pm \not{v})$. N_v and h_v correspond to the upper and lower components of a Dirac spinor and, thus, positive- and negative-energy solutions, respectively. The effects of the h_v components at low energies can be interpreted as contact terms so that the resulting

Lagrangian involves only N_v and its derivatives. Analogously, the Δ resonance is included by defining a "light" spin-3/2 and isospin-3/2 field

$$T_i^\mu = e^{im_N v\cdot x} P_v^+ \xi_{ij}^{3/2} \left(P_{33}^{3/2}\right)^{\mu\nu} \Psi_\nu^j, \tag{18}$$

with the spin and isospin projection operators $P_{33}^{3/2}$ and $\xi_{ij}^{3/2}$, respectively. The other "heavy" component is integrated out of the action. For more details on the HB expansion in the pion-nucleon-Δ sector the reader is referred to Refs. [16,17]. For the calculation at order ϵ^2, the required HB effective Lagrangian involves the following pieces:

$$\hat{\mathcal{L}}_{\rm eff} = \mathcal{L}_{\pi\pi}^{(2)} + \hat{\mathcal{L}}_{\pi N}^{(1)} + \hat{\mathcal{L}}_{\pi N}^{(2)} + \hat{\mathcal{L}}_{\pi\Delta}^{(1)} + \hat{\mathcal{L}}_{\pi\Delta}^{(2)} + \hat{\mathcal{L}}_{\pi N\Delta}^{(1)} + \hat{\mathcal{L}}_{\pi N\Delta}^{(2)}. \tag{19}$$

The explicit form of the nucleon terms can be found in Ref. [38], while the Δ terms are given in Ref. [16]. We emphasize, however, that the authors of Ref. [16], whose results for the HB effective Lagrangian are adopted in our work, made the choice for the gauge parameter $A = 0$ without specifying the values of the off-shell parameters. In order to be consistent with the convention used in the covariant calculations [see Eq. (11)], one has to choose in the HB framework

$$\hat{z} = -\tfrac{1}{2}, \quad \hat{g}_2 = -g_1, \quad \hat{g}_3 = -g_1 \tag{20}$$

(see Ref. [42] for more details).

III. INVARIANT AMPLITUDES

In this section we discuss the decomposition of the T matrix for the reaction $\pi N \to \pi\pi N$ in terms of the corresponding invariant amplitudes, following Ref. [35]. Throughout this work, the kinematical variables are defined as

$$\begin{aligned} &\pi^a(q_1)\, N(p = m_N v + k) \\ &\quad \to \pi^b(q_2)\, \pi^c(q_3)\, N'(p' = m_N v + k'), \end{aligned} \tag{21}$$

where N denotes a nucleon and π^a a pion with the isospin quantum number a.

A. Relativistic chiral perturbation theory

In the relativistic case, the T matrix can be expressed in terms of four invariant amplitudes F_i ($i \in \{1,2,3,4\}$), which depend on the five Mandelstam variables

$$\begin{aligned} &s = (p+q_1)^2, \quad s_1 = (q_2+p')^2, \quad s_2 = (q_3+p')^2, \\ &t_1 = (q_2-q_1)^2, \quad t_2 = (q_3-q_1)^2. \end{aligned} \tag{22}$$

The spin structure of the T matrix can be parametrized as

$$\begin{aligned} T_{ss'}^{abc} = {} & i\bar{u}^{(s')}\gamma_5 \big(F_1^{abc} + (\not{q}_2 + \not{q}_3)F_2^{abc} + (\not{q}_2 - \not{q}_3)F_3^{abc} \\ & + (\not{q}_2\not{q}_3 - \not{q}_3\not{q}_2)F_4^{abc}\big)u^{(s)}, \end{aligned} \tag{23}$$

where the superscripts on the spinors $\bar{u}, u$ refer to the spin. The isospin decomposition of the invariant amplitudes reads

$$F_i^{abc} = \chi_{N'}^\dagger \left(\tau^a\delta^{bc} B_i^1 + \tau^b\delta^{ac} B_i^2 + \tau^c\delta^{ab} B_i^3 + i\epsilon^{abc} B_i^4\right) \chi_N. \tag{24}$$

Here, the B_i's have the following symmetry under exchange of the two outgoing particles:

$$\begin{aligned} B_i^2(s,s_1,s_2,t_1,t_2) &= \epsilon_i B_i^3(s,s_2,s_1,t_2,t_1), \\ \epsilon_{1,2} = 1, \quad \epsilon_{3,4} &= -1. \end{aligned} \tag{25}$$

In the five physically accessible channels, the amplitudes contributing to each channel reduce to

$$\begin{aligned} &\text{I.} \quad \pi^- p \to \pi^0\pi^0 n : F_i = \sqrt{2} B_i^1, \\ &\text{II.} \quad \pi^- p \to \pi^+\pi^- n : F_i = \sqrt{2}\left(B_i^1 + B_i^2\right), \\ &\text{III.} \quad \pi^+ p \to \pi^+\pi^+ n : F_i = \sqrt{2}\left(B_i^2 + B_i^3\right), \\ &\text{IV.} \quad \pi^+ p \to \pi^+\pi^0 p : F_i = B_i^3 + B_i^4, \\ &\text{V.} \quad \pi^- p \to \pi^0\pi^- p : F_i = B_i^2 + B_i^4. \end{aligned} \tag{26}$$

The unpolarized invariant matrix element squared in the relativistic formalism has the form

$$|\mathcal{M}|^2 = \frac{1}{2}\sum_{s,s'} T_{ss'}^\dagger T_{ss'} = \sum_{i,j=1}^{4} \frac{y_{ij}}{4m_N^2} F_i^* F_j, \tag{27}$$

with the weight functions $y_{ij} = y_{ji}$ given by the trace over the respective Dirac structures (see the Appendix).

B. Heavy-baryon chiral perturbation theory

In the HB framework, the spin structure of an amplitude is given by a combination of the noncommuting Pauli-Lubanski spin vectors S_μ. In the case of $\pi N \to \pi\pi N$, the transition matrix can be written in terms of four invariant amplitudes, A, B, C, and D, which depend on the five momenta, k, k', q_1, q_2, and q_3, and are defined via [34]

$$\begin{aligned} T_{ss'}^{abc} = {} & \bar{u}_v^{(s')}\big(S\cdot q_1\, A^{abc} + S\cdot q_2\, B^{abc} + S\cdot q_3\, C^{abc} \\ & + i\epsilon_{\mu\nu\alpha\beta}\, q_1^\mu q_2^\nu q_3^\alpha v^\beta\, D^{abc}\big)u_v^{(s)}. \end{aligned} \tag{28}$$

Here, the HB spinor $u_v^{(s)}$ is given in the Pauli spinor representation,

$$u_v^{(s)}(p) = P_v^+ u^{(s)}(p) = \mathcal{N}\begin{pmatrix}\chi_s \\ 0\end{pmatrix}. \tag{29}$$

The normalization factor

$$\mathcal{N} = \sqrt{\frac{p^0 + m_N}{2m_N}} \tag{30}$$

ensures the proper matching to the relativistic theory and has to be taken into account in the $1/m_N$ expansion,

$$\mathcal{N}\mathcal{N}' = 1 + \mathcal{O}\left(\frac{1}{m_N^2}\right). \tag{31}$$

Thus, for a tree-level calculation, the normalization factors can be set equal to 1. The isospin decomposition is the same as in the relativistic case, namely,

$$\begin{aligned} X^{abc} &= \chi_{N'}^\dagger \left(\tau^a\delta^{bc} X_1 + \tau^b\delta^{ac} X_2 + \tau^c\delta^{ab} X_3 + i\epsilon^{abc} X_4\right)\chi_N, \\ X &\in \{A,B,C,D\}, \end{aligned} \tag{32}$$

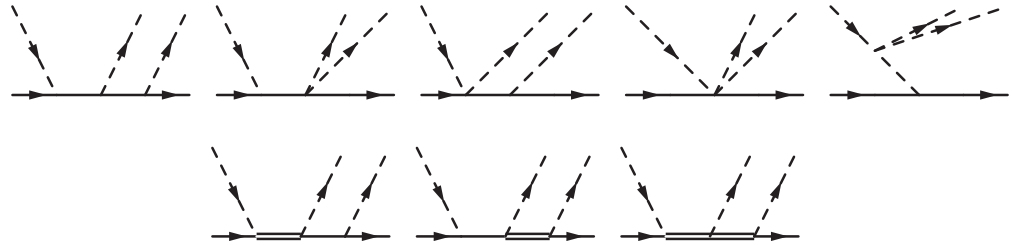

FIG. 1. LO graphs for the reaction $\pi N \to \pi\pi N$. Nucleons are denoted by solid lines; pions, by dashed lines. Δ is denoted by a double solid line. Crossed diagrams are not shown.

and thus the reduction in the five physically accessible channels is the same:

$$\begin{aligned}
&\text{I.} && \pi^- p \to \pi^0\pi^0 n : X = \sqrt{2}X_1,\\
&\text{II.} && \pi^- p \to \pi^+\pi^- n : X = \sqrt{2}(X_1 + X_2),\\
&\text{III.} && \pi^+ p \to \pi^+\pi^+ n : X = \sqrt{2}(X_2 + X_3),\\
&\text{IV.} && \pi^+ p \to \pi^+\pi^0 p : X = X_3 + X_4,\\
&\text{V.} && \pi^- p \to \pi^0\pi^- p : X = X_2 + X_4.
\end{aligned} \tag{33}$$

The unpolarized invariant matrix element squared in the HB formalism reads

$$\begin{aligned}
|\mathcal{M}|^2 &= \frac{1}{2}\sum_{s,s'} T^\dagger_{ss'} T_{ss'}\\
&= \frac{1}{4}\Big[|A|^2\boldsymbol{q}_1^2 + |B|^2\boldsymbol{q}_2^2 + |C|^2\boldsymbol{q}_3^2 + (A^*B + AB^*)\boldsymbol{q}_1\cdot\boldsymbol{q}_2\\
&\quad + (A^*C + AC^*)\boldsymbol{q}_1\cdot\boldsymbol{q}_3 + (B^*C + BC^*)\boldsymbol{q}_2\cdot\boldsymbol{q}_3\\
&\quad + 4|D|^2\boldsymbol{q}_1^2\boldsymbol{q}_2^2\boldsymbol{q}_3^2\big(1-x_1^2\big)\big(1-x_2^2\big)\\
&\quad \times\left(1 - \frac{(z - x_1x_2)^2}{\big(1-x_1^2\big)\big(1-x_2^2\big)}\right)\Big],
\end{aligned} \tag{34}$$

where x_1, x_2, and z are the cosines of the angles between $\boldsymbol{q}_1$ and $\boldsymbol{q}_2$, $\boldsymbol{q}_1$ and $\boldsymbol{q}_3$, and $\boldsymbol{q}_2$ and $\boldsymbol{q}_3$, respectively.

IV. TREE-LEVEL CONTRIBUTIONS TO THE SCATTERING AMPLITUDE

The LO and NLO diagrams emerging at orders ε^1 and ε^2 in the small-scale expansion in the relativistic framework are shown in Figs. 1 and 2, respectively. The LO diagrams are constructed solely from the lowest-order vertices and thus depend only on the well-known LECs F_π, g_A and the pion-nucleon-Δ axial constant h_A. Subleading diagrams involve a single insertion of the LEC c_i from $\mathcal{L}^{(2)}_{\pi N}$, which are known from pion-nucleon scattering, or b_i from $\mathcal{L}^{(2)}_{\pi N\Delta}$. We do not show diagrams involving an insertion of the LEC c_1^Δ, whose contributions are taken into account by using the physical values of the mass of the Δ isobar.

When performing the calculation within the HB framework, one needs to take into account additional diagrams involving $1/m_N$-vertices shown in Fig. 3. Notice that these vertices are fixed by the Poincaré invariance and do not involve any additional parameters.

We further emphasize that, given the fact that the Δ isobar is an unstable particle, it is not appropriate to use the free Δ propagator given in Eqs. (15) in the resonance region corresponding to $p^2 \sim m_\Delta^2$. In particular, dressing of the Δ becomes necessary, resumming all 1-Δ-irreducible diagrams, which obviously become large in the kinematical region with $p^2 - m_\Delta^2 = \mathcal{O}(M_\pi^2)$ (see Ref. [37] for details). Here we take this effect into account using the following simple expressions for the Δ propagator, where, in particular, the imaginary part of the derivative of the self-energy has been neglected (see Ref. [37]). In the relativistic framework it reads

$$\begin{aligned}
\mathcal{G}_\Delta^{\mu\nu}(p) = &-\frac{\not{p} + m_\Delta}{p^2 - m_\Delta^2 + \mathrm{i}m_\Delta\Gamma}\\
&\times\left(g^{\mu\nu} - \frac{1}{3}\gamma^\mu\gamma^\nu + \frac{1}{3}\frac{p^\mu\gamma^\nu - p^\nu\gamma^\mu}{m_\Delta} - \frac{2}{3}\frac{p^\mu p^\nu}{m_\Delta^2}\right),
\end{aligned} \tag{35}$$

with Γ being the decay width of the $\Delta(1232)$ resonance, while the expression in the HB framework has a simpler form:

$$\hat{\mathcal{G}}_\Delta^{\mu\nu}(p) = \frac{-1}{v\cdot k - \Delta + \frac{\mathrm{i}}{2}\Gamma}\big(P_{33}^{3/2}\big)^{\mu\nu}\xi^{ij}_{3/2}. \tag{36}$$

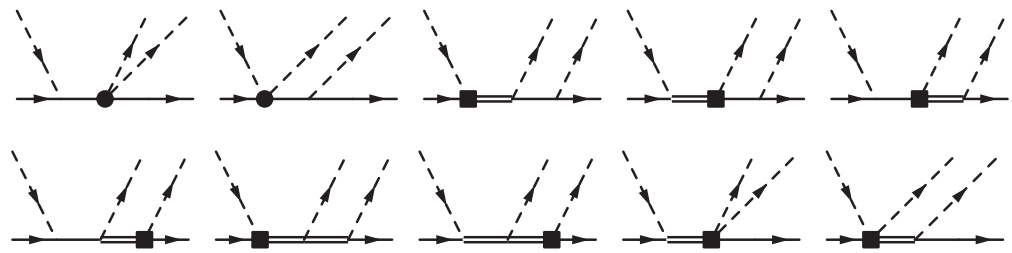

FIG. 2. NLO graphs for the reaction $\pi N \to \pi\pi N$. A filled circle (filled square) denotes an insertion of the c_i (b_i) vertices. Crossed diagrams are not shown.

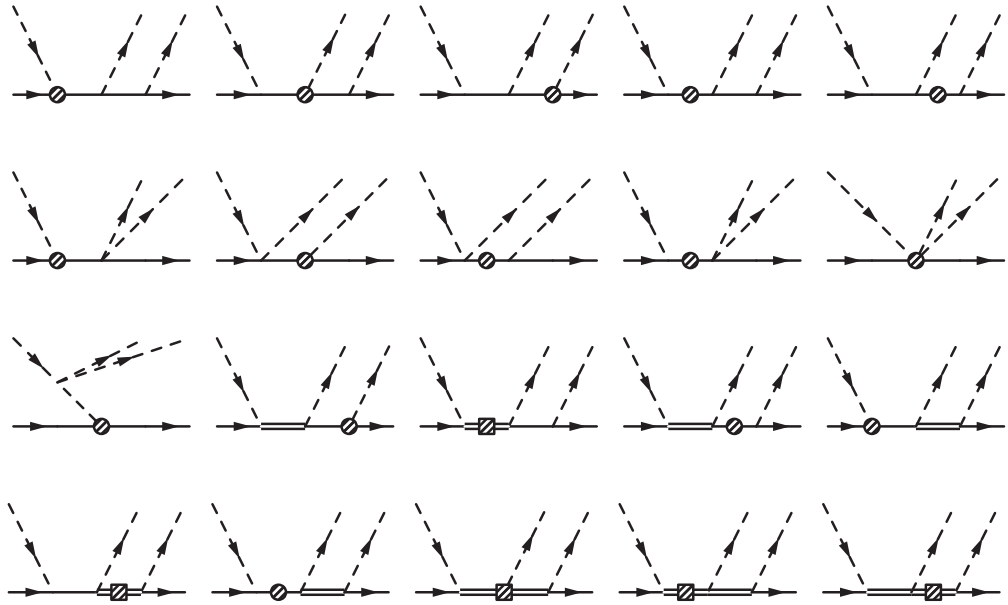

FIG. 3. Additional NLO graphs contributing to the reaction $\pi N \to \pi\pi N$ in the heavy-baryon framework. A hatched circle/square denotes a pure $1/m_N$ insertion. Crossed diagrams are not shown.

At the level of accuracy of our calculations this should be completely sufficient. In fact, in Ref. [26] the energy dependence of the width was incorporated. A more refined and consistent treatment of the Δ propagator will be done in a future work. See Ref. [43] for a related work.

While "dressing" of the Δ is, strictly speaking, only required in the resonance region, we use the expressions in Eqs. (35) and (36) for the Δ propagator in all diagrams and for all kinematical regions. Given that $\Gamma \sim \mathcal{O}(M_\pi^3)$, this procedure affects contributions to the amplitude at orders ϵ^3, which are beyond the scope of the present work.

For the nucleonic contributions to the scattering amplitude, the results within the covariant and HB frameworks we obtain agree with the ones published in Refs. [24,34]. The expressions for the Δ contributions to the amplitude are too involved to be given here but can be made available as a *Mathematica* notebook upon request.

V. OBSERVABLES

To match the conventions adopted by the experimentalists, one needs to calculate the differential cross sections with respect to different kinematical variables. In particular, there are differential cross sections with respect to the outgoing pion energies and solid angles. Thus, it is advantageous to express the integration variables in spherical coordinates and pion energies. There is a second set of differential cross sections, which are with respect to the kinematics of the final dipion system. These can be derived from the first set.

The experimentalists' convention suggests to choose the coordinate frame such that $\boldsymbol{q}_1$ defines the z-direction and $\boldsymbol{q}_2$ lies in the xz-plane so that, by construction, the azimuthal angle of π^b is zero [see Fig. 4(a)]. It is advantageous to introduce an auxiliary angle ϕ [see Fig. 4(b)], which is related to the

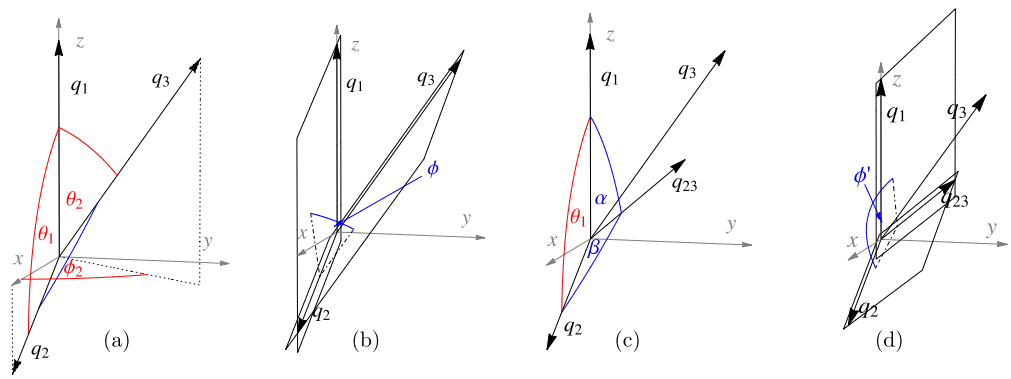

FIG. 4. (Color online) Kinematics and the definitions of angles θ_1, θ_2, and ϕ_2 (a), ϕ (b), α and β (c), and ϕ' (d).

azimuthal angles $x_i = \cos\theta_i$ via

$$x_2 = x_1 z + \sqrt{(1-x_1^2)(1-z^2)}\cos\phi. \tag{37}$$

The formulas for the total and the double- and triple-differential cross sections of the first set thus read

$$\begin{aligned}
\sigma &= \frac{4m_N^2\mathcal{S}}{(4\pi)^4\sqrt{s}|\boldsymbol{q}_1|}\int_{\omega_2^-}^{\omega_2^+}\mathrm{d}\omega_2\int_{\omega_3^-}^{\omega_3^+}\mathrm{d}\omega_3 \\
&\quad\times\int_{-1}^{1}\mathrm{d}x_1\int_0^{\pi}\mathrm{d}\phi\ |\mathcal{M}|^2, \\
\frac{\mathrm{d}^2\sigma}{\mathrm{d}\omega_2\mathrm{d}\Omega_2} &= \frac{8m_N^2\mathcal{S}}{(4\pi)^5\sqrt{s}|\boldsymbol{q}_1|}\int_{\omega_3^-}^{\omega_3^+}\mathrm{d}\omega_3\int_0^{\pi}\mathrm{d}\phi\ |\mathcal{M}|^2, \\
\frac{\mathrm{d}^3\sigma}{\mathrm{d}\omega_2\mathrm{d}\Omega_2\mathrm{d}\Omega_3} &= \frac{4m_N^2\mathcal{S}|\boldsymbol{q}_2||\boldsymbol{q}_3|}{(4\pi)^5\sqrt{s}|\boldsymbol{q}_1|\tilde{p}_0}|\mathcal{M}|^2,
\end{aligned} \tag{38}$$

where the integration limits are given by

$$\begin{aligned}
\omega_3^{\pm} &= \frac{1}{2\big(s-2\sqrt{s}\,\omega_2+M_\pi^2\big)} \\
&\quad\times\Big[(\sqrt{s}-\omega_2)\big(s-2\sqrt{s}\,\omega_2-m_N^2+2M_\pi^2\big) \\
&\quad\pm|\boldsymbol{q}_2|\sqrt{\big(s-2\sqrt{s}\,\omega_2-m_N^2\big)^2-4m_N^2M_\pi^2}\Big]
\end{aligned} \tag{39}$$

and

$$\omega_2^- = M_\pi, \quad \omega_2^+ = \frac{(\sqrt{s}-M_\pi)^2-m_N^2+M_\pi^2}{2(\sqrt{s}-M_\pi)}. \tag{40}$$

$\mathcal{S}$ is a Bose symmetry factor: $\mathcal{S}=1/2$ for identical outgoing pions and $\mathcal{S}=1$ otherwise. The kinematical variables in the center-of-mass system (CMS) are defined according to

$$\begin{aligned}
s &= (m_N+M_\pi)^2+2m_N T_\pi, \\
\omega_1 &= \frac{s+M_\pi^2-m_N^2}{2\sqrt{s}}, \\
s_1 &= s-2\sqrt{s}\,\omega_3+M_\pi^2, \\
s_2 &= s-2\sqrt{s}\,\omega_2+M_\pi^2, \\
t_1 &= 2\big(M_\pi^2-\omega_1\omega_2+\boldsymbol{q}_1\cdot\boldsymbol{q}_2\big), \\
t_2 &= 2\big(M_\pi^2-\omega_1\omega_3+\boldsymbol{q}_1\cdot\boldsymbol{q}_3\big), \\
|\boldsymbol{q}_2||\boldsymbol{q}_3|z &= \omega_2\omega_3-\sqrt{s}(\omega_2+\omega_3)+M_\pi^2+\frac{1}{2}\big(s-m_N^2\big),
\end{aligned} \tag{41}$$

where T_π is the kinetic energy of the incoming pion in the laboratory frame. Furthermore,

$$\tilde{p}_0 = \frac{\omega_3\left(\frac{1}{2}\big(s-m_N^2\big)-\sqrt{s}\,\omega_2\right)+M_\pi^2(\omega_2+\omega_3-\sqrt{s})}{\omega_3^2-M_\pi^2}. \tag{42}$$

Using the double- and triple-differential cross sections in Eq. (38), one defines the angular correlation function W as follows:

$$W = 4\pi\left(\frac{\mathrm{d}^3\sigma}{\mathrm{d}\omega_2\mathrm{d}\Omega_2\mathrm{d}\Omega_3}\Big/\frac{\mathrm{d}^2\sigma}{\mathrm{d}\omega_2\mathrm{d}\Omega_2}\right). \tag{43}$$

The second set of differential cross sections is with respect to the final dipion system with $q_{23}=q_2+q_3$ [see Fig. 4(c)]. Again, it is advantageous to define an auxiliary angle ϕ' [see Fig. 4(d)], which is related to x_1 via

$$x_1 = \cos\beta\cos\alpha+\sqrt{(1-\cos^2\alpha)(1-\cos^2\beta)}\cos\phi'. \tag{44}$$

Denoting the final dipion mass $M_{\pi\pi}^2$, the scattering angle of the two outgoing pions in the CMS of the final dipion θ, and with $t=(q_1-q_2-q_3)^2$, the differential cross sections read

$$\begin{aligned}
\frac{\mathrm{d}\sigma}{\mathrm{d}M_{\pi\pi}^2} &= \frac{m_N^2\mathcal{S}}{(4\pi)^4 s|\boldsymbol{q}_{23}||\boldsymbol{q}_1|^2}\int\mathrm{d}t\int\mathrm{d}\omega_2\int_0^{\pi}\mathrm{d}\phi'\ |\mathcal{M}|^2, \\
\frac{\mathrm{d}\sigma}{\mathrm{d}t} &= \frac{m_N^2\mathcal{S}}{(4\pi)^4 s|\boldsymbol{q}_1|^2}\int\frac{\mathrm{d}M_{\pi\pi}^2}{|\boldsymbol{q}_{23}|}\int\mathrm{d}\omega_2\int_0^{\pi}\mathrm{d}\phi'\ |\mathcal{M}|^2, \\
\frac{\mathrm{d}\sigma}{\mathrm{d}M_{\pi\pi}^2\mathrm{d}t} &= \frac{m_N^2\mathcal{S}}{(4\pi)^4 s|\boldsymbol{q}_{23}||\boldsymbol{q}_1|^2}\int\mathrm{d}\omega_2\int_0^{\pi}\mathrm{d}\phi'\ |\mathcal{M}|^2, \\
\frac{\mathrm{d}\sigma}{\mathrm{d}\cos\theta} &= \frac{2m_N^2\mathcal{S}}{(4\pi)^4 s|\boldsymbol{q}_1|^2}\int\mathrm{d}M_{\pi\pi}^2\int\mathrm{d}\cos\alpha \\
&\quad\times\int\mathrm{d}\omega_2\,\frac{|\mathcal{M}|^2|\boldsymbol{q}_1'||\boldsymbol{q}_2'|}{|\boldsymbol{q}_2|\sin\phi'\sqrt{(1-\cos^2\alpha)(1-\cos^2\beta)}}.
\end{aligned} \tag{45}$$

The integration boundaries for t are given by

$$\begin{aligned}
t^{\pm} &= M_\pi^2+M_{\pi\pi}^2-2\omega_1\omega_{23}\pm 2|\boldsymbol{q}_1||\boldsymbol{q}_{23}| \quad \text{with} \\
\omega_{23} &= \omega_2+\omega_3 = \frac{M_{\pi\pi}^2+s-m_N^2}{2\sqrt{s}}.
\end{aligned} \tag{46}$$

The integration boundaries for ω_2 are restricted to the overlap of the interval $[\omega_2^-,\omega_2^+]$ from Eq. (40) and the interval $[\tilde{\omega}_2^-,\tilde{\omega}_2^+]$ with

$$\tilde{\omega}_2^{\pm} = \frac{\omega_{23}}{2}\pm\sqrt{\frac{\big(\omega_{23}^2-M_{\pi\pi}^2\big)\big(M_{\pi\pi}^2-4M_\pi^2\big)}{4M_{\pi\pi}^2}}. \tag{47}$$

The integration boundaries for $M_{\pi\pi}^2$ are

$$\begin{aligned}
M_{\pi\pi}^{2\pm} &= \frac{1}{m_N^2}\Bigg(\frac{t}{2}\big(s+m_N^2-M_\pi^2\big)+m_N^2M_\pi^2 \\
&\quad\pm|\boldsymbol{q}_1|\sqrt{-s\,t\big(4m_N^2-t\big)}\Bigg)
\end{aligned} \tag{48}$$

and also $M_{\pi\pi}^2\in(4M_\pi^2,(\sqrt{s}-m_N)^2)$. Finally, the integration for the differential cross section with respect to the scattering angle is restricted by the condition $\sin\phi'<1$. Furthermore, the magnitudes of the pion momenta in the dipion CMS are

$$\begin{aligned}
|\boldsymbol{q}_1'|^2 &= \frac{M_{\pi\pi}^4-2M_{\pi\pi}^2\big(t+M_\pi^2\big)+\big(t-M_\pi^2\big)^2}{4M_{\pi\pi}^2}, \\
|\boldsymbol{q}_2'|^2 &= \frac{M_{\pi\pi}^2-4M_\pi^2}{4}.
\end{aligned} \tag{49}$$

VI. FITTING PROCEDURE

The scattering amplitude for the reaction $\pi N\to\pi\pi N$ depends on several LECs as explained in Sec. IV. Throughout this work, we use the following values for the various LECs and masses entering the LO effective Lagrangian: $M_\pi = 139.57$ MeV, $F_\pi = 92.4$ MeV, $m_N = 938.27$ MeV, $g_A = 1.26$,

TABLE I. LEC c_i from the pion-nucleon sector for two fits in a Δ-full and Δ-less theory. All values are given in GeV^{-1}.

	c_1	c_2	c_3	c_4
		(a) Δ-full χPT		
KH	−0.95	1.90	−1.78	1.50
GW	−1.41	1.84	−2.55	1.87
		(b) Δ-less χPT		
KH	−0.75	3.49	−4.77	3.34
GW	−1.13	3.69	−5.51	3.71

$\Delta = 294$ MeV, $\Gamma = 118$ MeV. For the $\pi N\Delta$ axial coupling constant h_A, we adopt the same value as used in Ref. [42], namely $h_A = 1.34$, corresponding to the large-N_c prediction. Note that this value is close to the one determined from the width of the Δ resonance (in the covariant framework). At NLO we encounter contributions proportional to the LEC c_i's from $\mathcal{L}^{(2)}_{\pi N}$. Since we intend to investigate, among others, the role played by the Δ isobar by comparing the results obtained within the Δ-less and Δ-full formulations of chiral EFT, we adopt here the values of the c_i's determined from the fits to pion-nucleon scattering in Refs. [42,44] and collected in Table I. These fits have been performed to the partial-wave analyses of the group at George Washington University (GW) [45] and the Karlsruhe-Helsinki analysis (KH) [46] at the subleading one-loop order of HBχPT with and without explicit Δ and using the same values of various parameters as specified above. The values for the Δ-less approach are consistent with the theoretically cleaner determination from inside the Mandelstam triangle [47]. Thus, given that the values of the LEC c_i's are fixed, there are no free parameters in the Δ-less approach at order q^2.

It should be emphasized that the values of c_i's adopted in our study are taken from fits to πN phase shifts carried out at a higher order, namely, q^4 ($\epsilon^3 + q^4$), within the Δ-less (Δ-full) HB approach.[2] The values of c_i's determined from πN scattering are known to change strongly (moderately) when going from the order q^2 to q^3 (q^3 to q^4), indicating a large theoretical uncertainty due to truncation of the chiral expansion at the tree level. Given that the main focus of our work is to compare predictions for the reaction $\pi N \to \pi\pi N$ based on different theoretical formulations, we refrain from a detailed discussion of the accuracy of our calculations and, in particular, of the sensitivity to the values of c_i's. This issue will be addressed in an upcoming publication where the calculations will be extended to the one-loop level.

Further LECs contribute to the amplitude in the Δ-full approach at order ε^2. In particular, in addition to the c_i's from $\mathcal{L}^{(2)}_{\pi N}$, there are also contributions involving the LECs b_3, b_4, b_5, and b_6 from $\mathcal{L}^{(2)}_{\pi N\Delta}$ and g_1 from $\mathcal{L}^{(1)}_{\pi\Delta}$, whose determination is discussed below. Note that there is a large-N_c prediction for the leading-order pion-Δ coupling constant g_1, namely,

$$g_1 = \tfrac{9}{5} g_A = 2.27, \tag{50}$$

which is used in some fits as described below.

Isospin breaking is accounted for in a minimal way by shifting T_π from the isospin symmetric threshold to the physical threshold of each channel [35]. In the laboratory frame, the incoming pion kinetic energy at threshold is

$$T_\pi^{\rm thr} = \frac{(M_{\pi^b} + M_{\pi^c} + m'_N)^2 - (m_N + M_{\pi^a})^2}{2m_N}, \tag{51}$$

whereas the isospin symmetric case ($m'_N = m_N$, $M_{\pi^a} = M_{\pi^b} = M_{\pi^c} = M_\pi$) yields

$$T_\pi^{\rm thr,iso} = M_\pi \left(1 + \frac{3M_\pi}{2m_N}\right) = 170.71 \text{ MeV}. \tag{52}$$

The resulting shifts $\delta T_\pi = T_\pi^{\rm thr} - T_\pi^{\rm thr,iso}$ for each channel are thus

$$\begin{aligned}
&\text{I.} && \pi^- p \to \pi^0\pi^0 n : \delta T_\pi = -10.21 \text{ MeV},\\
&\text{II.} && \pi^- p \to \pi^+\pi^- n : \delta T_\pi = +1.68 \text{ MeV},\\
&\text{III.} && \pi^+ p \to \pi^+\pi^+ n : \delta T_\pi = +1.68 \text{ MeV},\\
&\text{IV.} && \pi^+ p \to \pi^+\pi^0 p : \delta T_\pi = -5.95 \text{ MeV},\\
&\text{V.} && \pi^- p \to \pi^0\pi^- p : \delta T_\pi = -5.95 \text{ MeV}.
\end{aligned} \tag{53}$$

All fits described below are performed globally to the experimental data in all five channels simultaneously. For the fitting procedure, only the total cross-section data were used, which are taken from the compilation [48] and from [49,50,51]. The χ^2 is given by the square of the difference between our calculated values of the total cross section and the experimental central values divided by the squared errors on the latter. Typically a very good fit corresponds to a χ^2 per degree of freedom (χ^2/dof) close to 1.

A. Heavy-baryon chiral perturbation theory

Given the expected validity range of HBχPT, only data with $T_\pi < 250$ MeV were used in the fits. The choice of this still rather high energy is motivated by the fact that in some channels there are essentially no data in the very-near-threshold region.

In the static limit, the LECs b_3 and b_6 are redundant because they can be fully absorbed into shifts of other LECs [52],

$$\begin{aligned}
h_A &\to h_A - \Delta\,(b_3 + b_6),\\
c_2 &\to c_2 + \tfrac{8}{9} h_A\,(b_3 + b_6),\\
c_3 &\to c_3 - \tfrac{8}{9} h_A\,(b_3 + b_6),\\
c_4 &\to c_4 + \tfrac{4}{9} h_A\,(b_3 + b_6),\\
b_4 &\to b_4 + \left(\tfrac{13}{9} g_1 - g_A\right)(b_3 + b_6),\\
b_5 &\to b_5 - \tfrac{4}{3} g_1\,(b_3 + b_6),
\end{aligned} \tag{54}$$

[2] Furthermore, the analyses in Refs. [42,44] are performed assuming that the nucleon mass scales as $m_N \sim \Lambda_\chi^2/M_\pi$, as commonly done in few-nucleon studies. This counting rule differs from the standard one, $m_N \sim \Lambda_\chi$, usually adopted in the single-nucleon sector, and also used in the present work, and leads to a stronger suppression of $1/m_N$ corrections. The impact of this inconsistency is irrelevant at the level of accuracy of our calculations.

TABLE II. LECs determined from global fits to the total cross-section data at NLO using the KH set of LEC c_i's from Table I(a) as input. A superscript asterisk indicates that the corresponding value is kept fixed. Values of LEC b_i are given in GeV^{-1}.

Fit with KH c_i's	g_1	b_4+b_5	b_4-b_5	b_3+b_6	b_3-b_6	χ^2/dof
HB approach						
$T_\pi < 250$ MeV	1.36±0.73	16.61 ± 0.66	-1.75 ± 9.78	–	–	9.42
	2.27*	16.00 ± 0.37	-7.99 ± 5.71	–	–	9.63
Relativistic						
$T_\pi < 250$ MeV	1.68±1.38	5.05 ± 0.39	-12.08 ± 15.59	0.08 ± 1.39	-1.02 ± 8.40	3.36
	2.27*	4.97 ± 0.29	-17.71 ± 12.22	0.39 ± 0.86	1.60 ± 7.62	3.40
$T_\pi < 400$ MeV	1.41±0.22	4.35 ± 0.08	1.62 ± 1.87	-1.07 ± 0.18	3.14 ± 1.61	4.26
	2.27*	4.51 ± 0.12	1.17 ± 1.61	-1.17 ± 0.12	7.36 ± 2.03	4.66

which is equivalent to setting $b_3 = -b_6$ in the amplitudes as done in Ref. [42]. Thus, the only free parameters one is left with at NLO are g_1, b_4, and b_5.

B. Relativistic chiral perturbation theory

In this case, we have carried out the fits using the same energy interval as in the HB approach, $T_\pi < 250$ MeV, as well as the larger energy range of $T_\pi < 400$ MeV. Note that, contrary to the HB formulation, the LECs b_3 and b_6 are no longer redundant at order ε^2 and have to be determined from the data, so that one is left with a total of five unknown parameters. Furthermore, given that we employ here the values of the LECs c_i of Ref. [42] as input in our analysis and in order to ensure a meaningful comparison with the HBχPT results, we have to account for the shifts induced in the LECs h_A, $c_{2,3,4}$, and $b_{4,5}$ by the nonvanishing linear combination $b_3 + b_6$ as specified in Eq. (54).

C. Results

At NLO several fits were performed, both with a free and with a fixed value of g_1. The results with the c_i's taken from the upper row in Table I(a) (KH) are summarized in Table II.

In all cases, we find that the LECs b_4 and b_5 are strongly anticorrelated. This is visualized in Fig. 5 for the HB approach and in the left panel in Fig. 6 for the relativistic calculation. As a result, while the value of the linear combination $b_4 + b_5$ can be reliably extracted in each fit, there is a very large uncertainty, about 100%, for the linear combination $b_4 - b_5$. Further, the LECs b_3 and b_6 also appear to be strongly anticorrelated in the relativistic approach as shown in the right panel in Fig. 6.

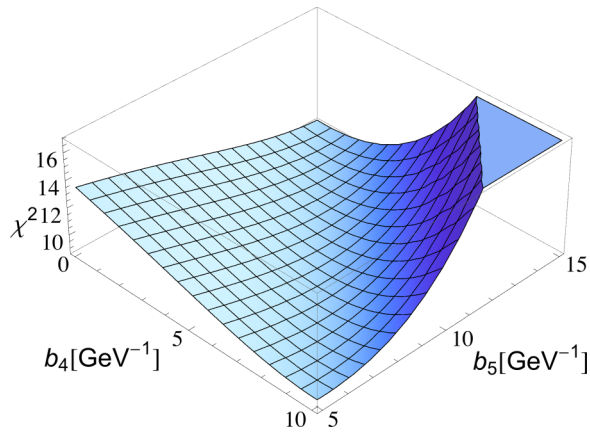

FIG. 5. (Color online) Fit in HBχPT: anticorrelation between b_4 and b_5 ($g_1 = 2.27$).

The significance of relativistic effects in the reaction $\pi N \to \pi\pi N$ is clearly seen in the strong reduction of χ^2/dof from ~9.5 in the HB approach to ~3.4 in relativistic χPT. In addition, the unnaturally large value of the linear combination $b_4 + b_5$, $b_4 + b_5 \sim 16$ GeV^{-1}, in HBχPT indicates that the energies up to $T_\pi = 250$ MeV employed in the fit are probably beyond the applicability range of the order-ϵ^2 HB approximation. In contrast, the fits carried out within the relativistic χPT framework lead to reasonably natural values for $b_4 + b_5$.

In order to test the stability of our results and to get further insights into the applicability range of relativistic χPT, we have extended the energy range used in the fits up to $T_\pi = 400$ MeV (see the last two rows in Table II). Remarkably, including the higher-energy data only increased the value of χ^2/dof by about 30%. As expected, including higher energies in the fit stabilizes the results for the LECs, which manifests itself in the significantly reduced error bars. It is comforting to see that the values of all LECs extracted from the unconstrained fits up to $T_\pi = 250$ MeV and $T_\pi = 400$ MeV agree with each other within the error bars. One also observes that the anticorrelations between the LECs b_4 and b_5 as well as b_3 and b_6 are much less pronounced in the higher-energy fit. The situation is similar in the constrained fits, although the deviations between the extracted LECs tend to be somewhat larger.

We further observe that there is a fairly minor sensitivity to the LEC g_1. In particular, fixing g_1 to its large-N_C value appears to only mildly affect the χ^2/dof and also has little impact on the extracted values of other LECs. This manifests itself in rather large error bars for g_1 when performing fits up to $T_\pi = 250$ MeV. The extracted values in the HB approach, $g_1 = 1.36 \pm 0.73$, and relativistic χPT, $g_1 = 1.68 \pm 1.38$, agree well with each other as well as with the large-N_c value of $g_1 = 2.27$. The higher-energy fit within the relativistic framework yields a similar result but with reduced error bars, $g_1 = 1.41 \pm 0.22$, which is somewhat smaller than the large-N_c prediction. It should, however, be emphasized that it is not completely consistent to fit g_1 while, at the same time,

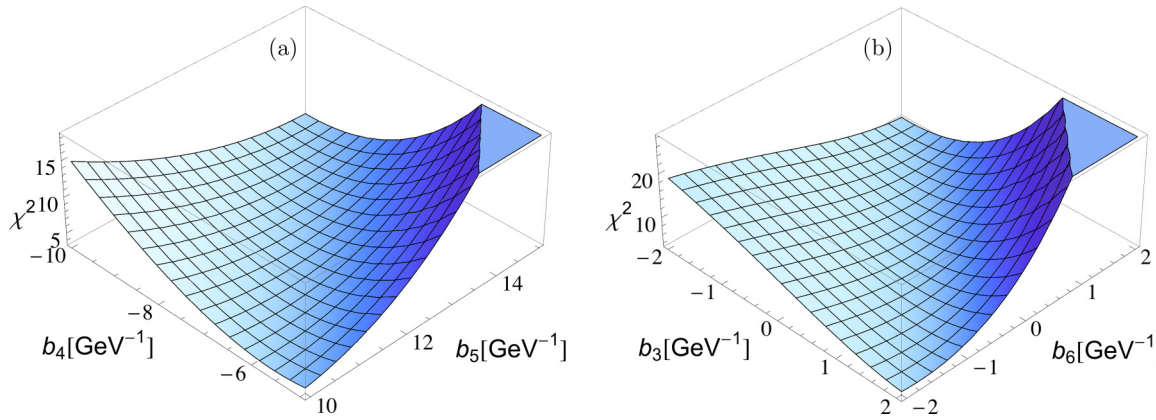

FIG. 6. (Color online) Fit in χPT: anticorrelation between b_4 and b_5 (a) ($g_1 = 2.27$, $b_3 = 0.99$ GeV^{-1}, $b_6 = -0.61$ GeV^{-1}) and between b_3 and b_6 (b) ($g_1 = 2.27$, $b_4 = -6.37$ GeV^{-1}, $b_5 = 11.34$ GeV^{-1}).

using the values for the LEC c_1 as input, which have been extracted from πN scattering in Ref. [42] using g_1 fixed to its large-N_c value. This could be improved in the future by carrying out a simultaneous analysis of the $\pi N \to \pi N$ and $\pi N \to \pi\pi N$ reactions.

Last but not least, we have also carried out fits using the GW set of c_i's from Table I, which lead to slightly different values for the fitted parameters without affecting any of the conclusions. The LECs resulting from the constrained fits up to $T_\pi = 250$ MeV using the KH and GW sets of LEC c_i's as input are listed in Table III.

VII. PREDICTIONS

We are now in the position to make predictions for various observables. Here and in what follows, we use the values of the LECs collected in Table III. This allows us to make a meaningful comparison between the predictions in the HB and those in the relativistic χPT. We also use both the KH and the GW sets of the LEC c_i from Table I in order to estimate the uncertainty associated with the pion-nucleon system which provides input for our calculations. Thus, all predictions at NLO (Q^2 or ϵ^2) are visualized by bands whose width corresponds to the variation of the LEC c_i between the KH and the GW values. Further, while we have analyzed all available low-energy observables in this reaction, we only show selected representative examples in the following.

The predictions for the total cross sections with incoming pion energies up to 400 MeV are presented in Fig. 7, in both the Δ-full and the Δ-less theories. The Δ-less calculations were performed with the c_i's taken from Table I(b). As can be seen, the relativistic approach describes the data at higher energies much better than the HB one, which is fully in line with the observations made in the previous section. The predictions within HBχPT at NLO appear to significantly underestimate the data in almost every channel, whereas the Δ-full HB predictions overshoot the cross sections for $T_\pi > 300$ MeV. The inclusion of the Δ in the relativistic case is mainly noticeable in the upper two channels, whereas the description of the other three channels is similar.

The HB approach also fails to describe various differential cross sections at NLO, most noticeably the double-differential cross section with respect to the solid angle Ω_2 and the pion kinetic energy $T_2 = \omega_2 - M_\pi$ in the channel $\pi^- p \to \pi^+\pi^- n$. The data for this observable are reported in Ref. [53] and the comparison between the predictions of relativistic and HB χPT are presented in Fig. 8. While the inclusion of the Δ in the HB formulation at order ϵ^2 shifts the theoretical results towards the data, these shifts are too small and are unable to bring the theory in agreement with the data. We emphasize, however, that the data are well described by the next-to-next-to-leading order (Q^3) Δ-less HB calculation in Ref. [34]. The relativistic Δ-full approach is able to describe the data properly already at NLO. Moreover, even the Δ-less covariant formulation yields a reasonably good description of the data at this order. The description of the data is somewhat better in χPT with explicit Δ except for the cross section at $\sqrt{s} = 1262$ MeV and the largest value of the kinetic energy of π^+, $T_2 = 31.4$ MeV.

TABLE III. LECs determined from global fits to the total cross-section data at NLO using the KH and GW sets of LECs c_i from Table I as input. A superscript asterisk indicates that the corresponding value is kept fixed. Values of LECs b_i are given in GeV^{-1}.

Fit	c_i	g_1	$b_4 + b_5$	$b_4 - b_5$	$b_3 + b_6$	$b_3 - b_6$	χ^2/dof
HB approach							
$T_\pi < 250$ MeV	KH	2.27*	16.00 ± 0.37	-7.99 ± 5.72	–	–	9.63
	GW	2.27*	15.99 ± 0.37	-8.42 ± 5.77	–	–	9.65
Relativistic							
$T_\pi < 250$ MeV	KH	2.27*	4.97 ± 0.29	-17.71 ± 12.22	0.39 ± 0.86	1.60 ± 7.62	3.40
	GW	2.27*	4.34 ± 0.29	-18.24 ± 10.77	0.70 ± 0.76	1.41 ± 6.38	3.47

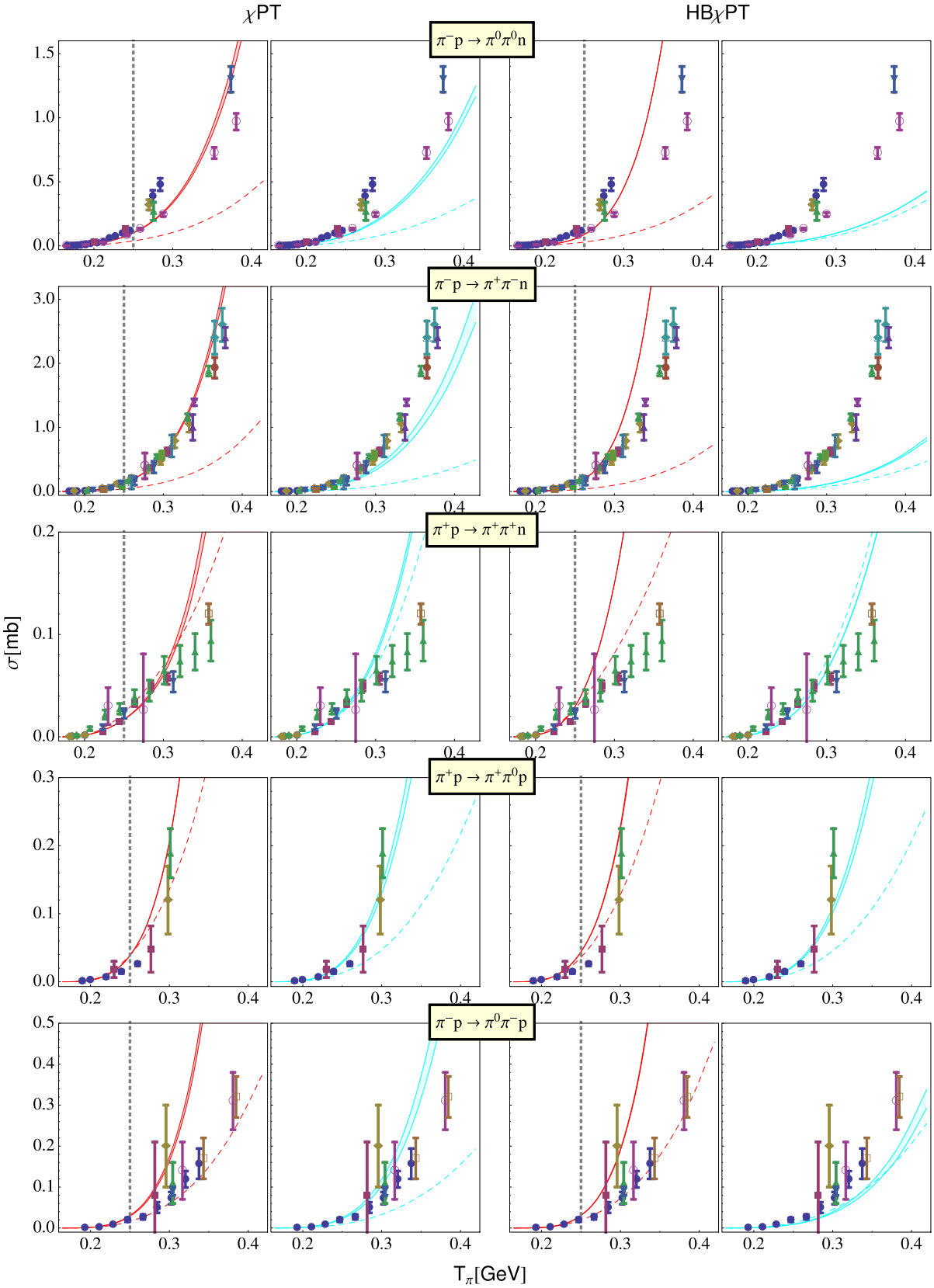

FIG. 7. (Color online) Predictions for the total cross section up to $T_\pi \simeq 400$ MeV. Columns from left to right correspond to the Δ-full covariant χPT, Δ-less covariant χPT, Δ-full HBχPT, and Δ-less HBχPT predictions, respectively. Dashed and solid lines refer to LO (i.e., order Q^1 or ϵ^1) and NLO (i.e., up to order Q^2 or ε^2) results. Energies used in the fit at NLO are below the vertical dotted line. Bands at NLO correspond to use of the KH and GW sets of LECs c_i.

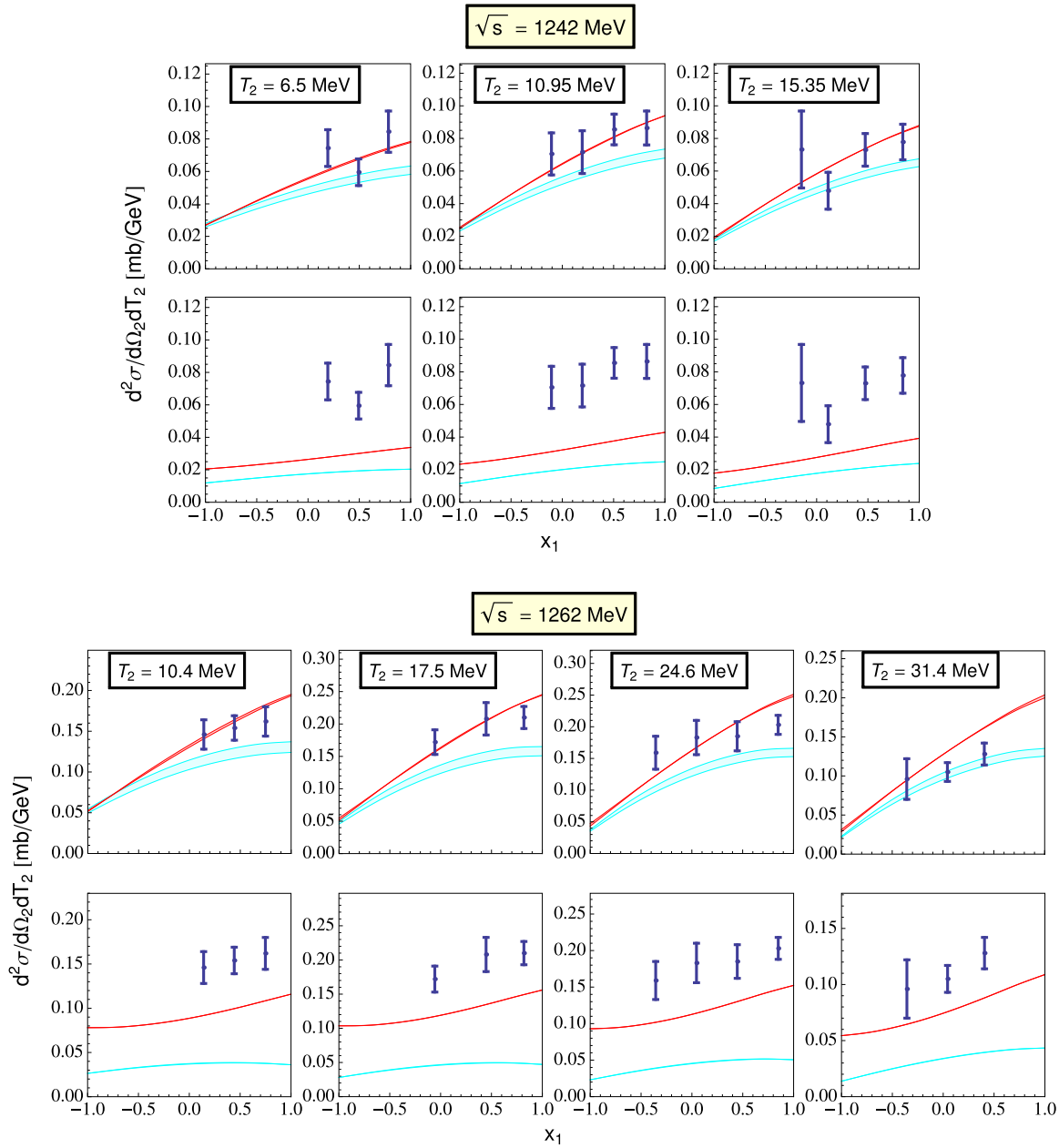

FIG. 8. (Color online) NLO χPT predictions for the double-differential cross sections for $\pi^- p \to \pi^+\pi^- n$ with respect to the kinetic energy and the solid angle of the outgoing π^+; see Eq. (38). Upper and lower panels correspond to the relativistic and heavy-baryon approaches, respectively. Light-gray (blue) and dark-gray (red) bands (the latter nearly shrink to lines) refer to Δ-less and Δ-full calculations, respectively. Bands correspond to use of the KH and GW sets of LECs c_i.

Given the failure of the NLO HB approach for the double-differential cross sections, we leave out the HB predictions in what follows and focus entirely on the results based on the relativistic framework. First, we consider the angular correlation function W defined in Eq. (43) in the channel $\pi^- p \to \pi^+\pi^- n$. Figure 9 (Figure 10) shows our NLO predictions in the Δ-less and Δ-full relativistic approaches in comparison with experimental data taken from Ref. [54] for fixed θ_1 and θ_2 (θ_1 and ϕ_2). One observes that the Δ-full results tend to have a stronger curvature, which, in most cases, is in better qualitative agreement with the shape of the experimental data. Generally, the data are reasonably well described in both approaches (given that the calculations are carried out at NLO in the low-energy expansion). The largest deviations between the ϵ^2 results and the data emerge at the lowest values of θ_2 and $\theta_1 = 39.0^\circ \ldots 41.5^\circ$ (see Fig. 9). In fact, the predictions of the Δ-less framework appear to be closer to the data in these cases (although the shape of the data is better described in the Δ-full theory). Given that these cases correspond to the largest differences between the Q^2 and the ϵ^2 results, and their magnitude is comparable with the deviation from the data, it is conceivable that higher-order corrections might be significant under these kinematical conditions.

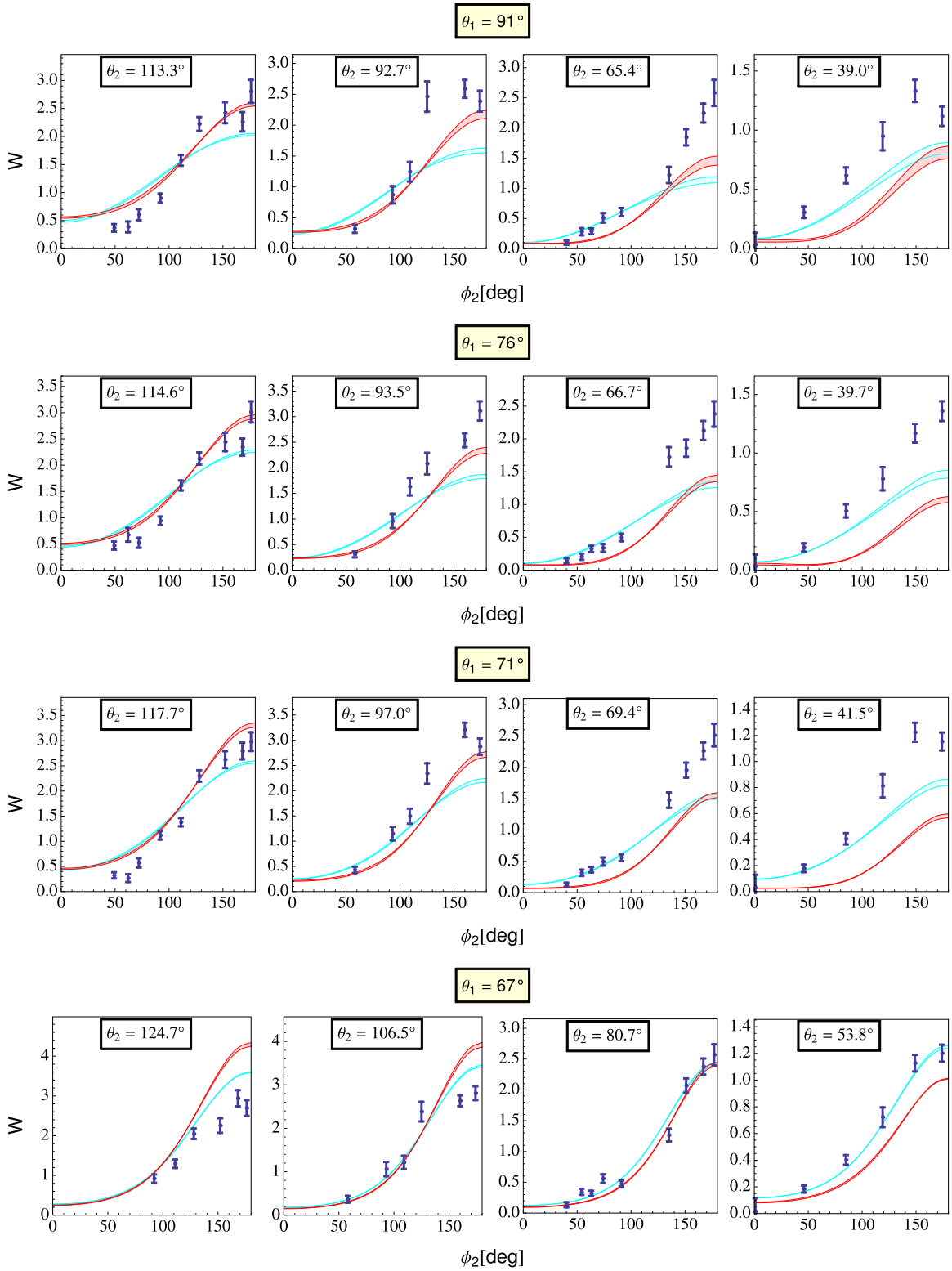

FIG. 9. (Color online) NLO relativistic χPT predictions for the angular correlation functions in the $\pi^- p \to \pi^+\pi^- n$ channel at fixed θ_1 and θ_2 for $\sqrt{s} = 1301$ MeV; see Eq. (43). Light-gray (blue) and dark-gray (red) bands refer to Δ-less and Δ-full calculations, respectively. Bands correspond to use of the KH and GW sets of LEC c_i.

We next turn to the single-differential cross sections with respect to $M^2_{\pi\pi}$ and t [see Eq. (45)]. Our predictions for $d\sigma/dM^2_{\pi\pi}$ and $d\sigma/dt$ are shown in comparison with the experimental data from Ref. [49] in the left and right panels in Fig. 11, respectively. In each case we compare the two channels, namely, $\pi^- p \to \pi^+\pi^- n$ and $\pi^+ p \to \pi^+\pi^+ n$.

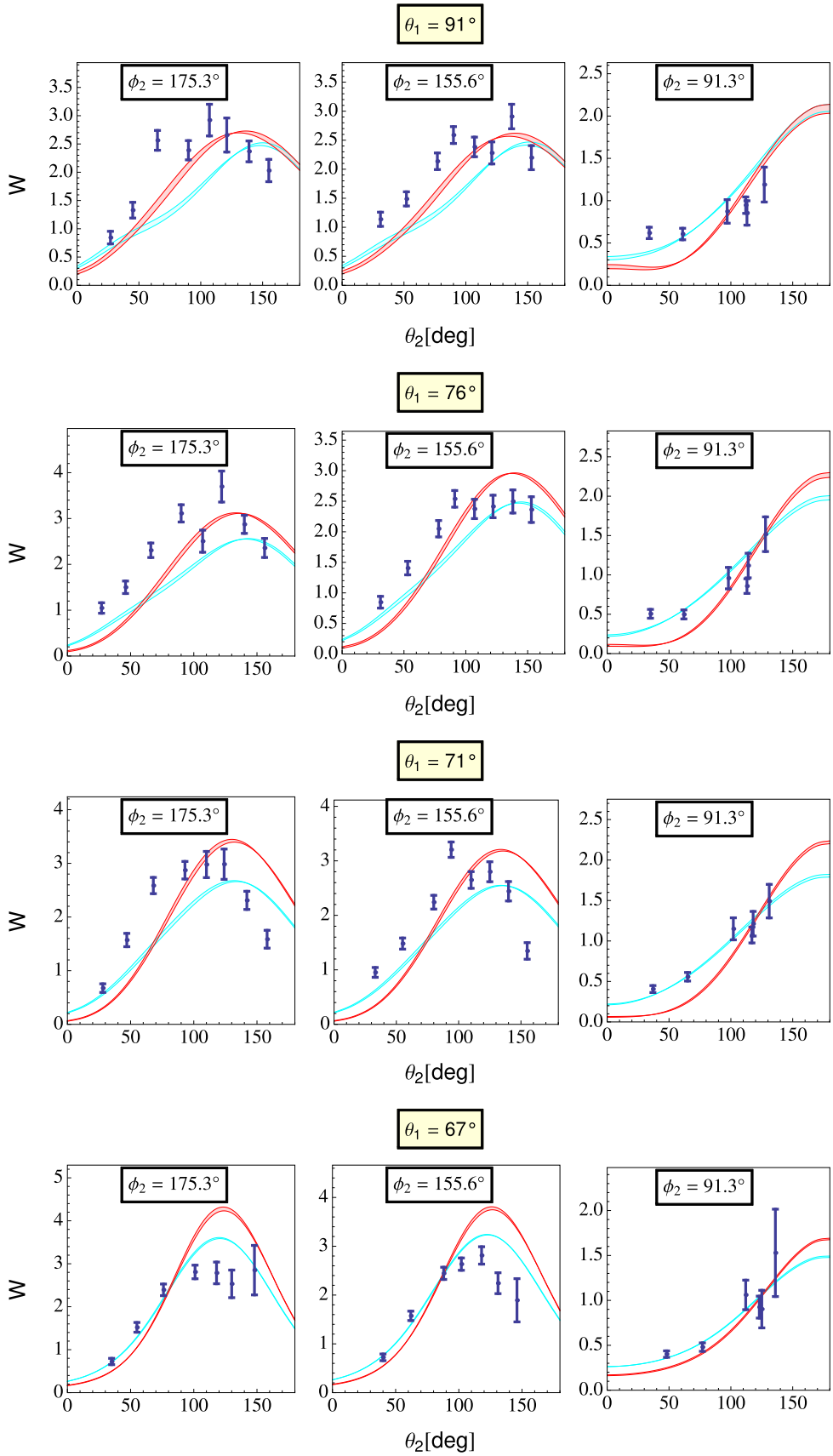

FIG. 10. (Color online) Comparison of NLO relativistic Δ-full and Δ-less χPT predictions for the angular correlation functions in the $\pi^- p \to \pi^+ \pi^- n$ channel at fixed θ_1 and ϕ_2 for $\sqrt{s} = 1301$ MeV; see Eq. (43). For remaining notation see the caption to Fig. 9.

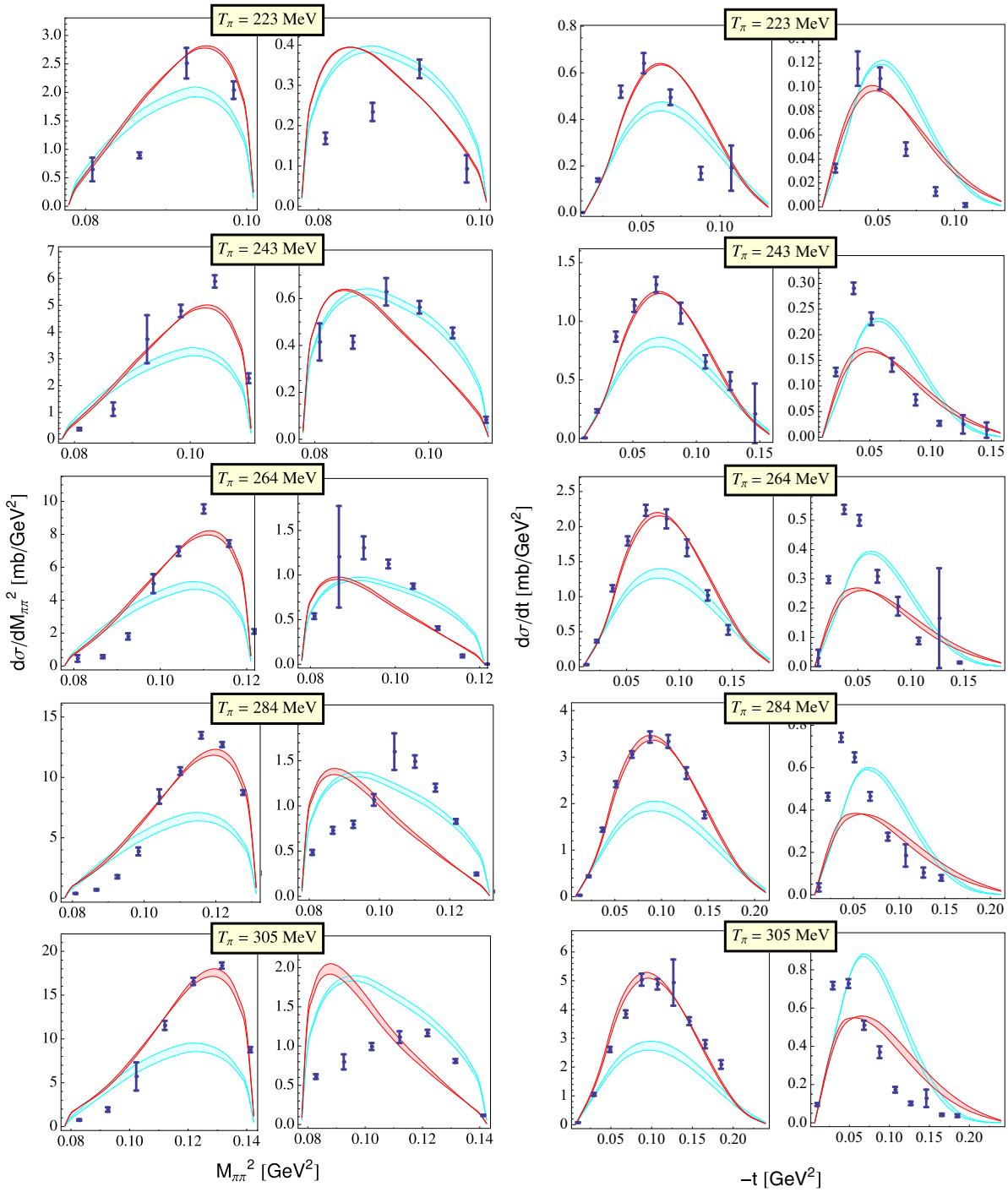

FIG. 11. (Color online) Comparison of NLO relativistic Δ-full and Δ-less χPT predictions for the single-differential cross sections with respect to $M_{\pi\pi}^2$ and t, respectively, between the two channels $\pi^- p \to \pi^+\pi^- n$ (left) and $\pi^+ p \to \pi^+\pi^+ n$ (right); see Eq. (45). For remaining notation see the caption to Fig. 9.

We recall that the total cross section is very accurately predicted at order ϵ^2 in the $\pi^+\pi^-$ channels (see Fig. 7). It is comforting to see that both single-differential cross sections are also well described in the Δ-full approach. On the other hand, Δ-less results at order Q^2 strongly underpredict the experimental data, which is in line with the observed underprediction of the total cross section. This is the most pronounced example of the importance of the explicit inclusion of the Δ isobar we found in our analysis. In the $\pi^+\pi^+$ channel, the single-differential cross sections are found to be poorly described at both Q^2 and ϵ^2 orders. In particular, even the shape of the cross section $d\sigma/dM_{\pi\pi}^2$ is not correctly reproduced. The situation is slightly better for the cross section $d\sigma/dt$. The observed large deviations from the data

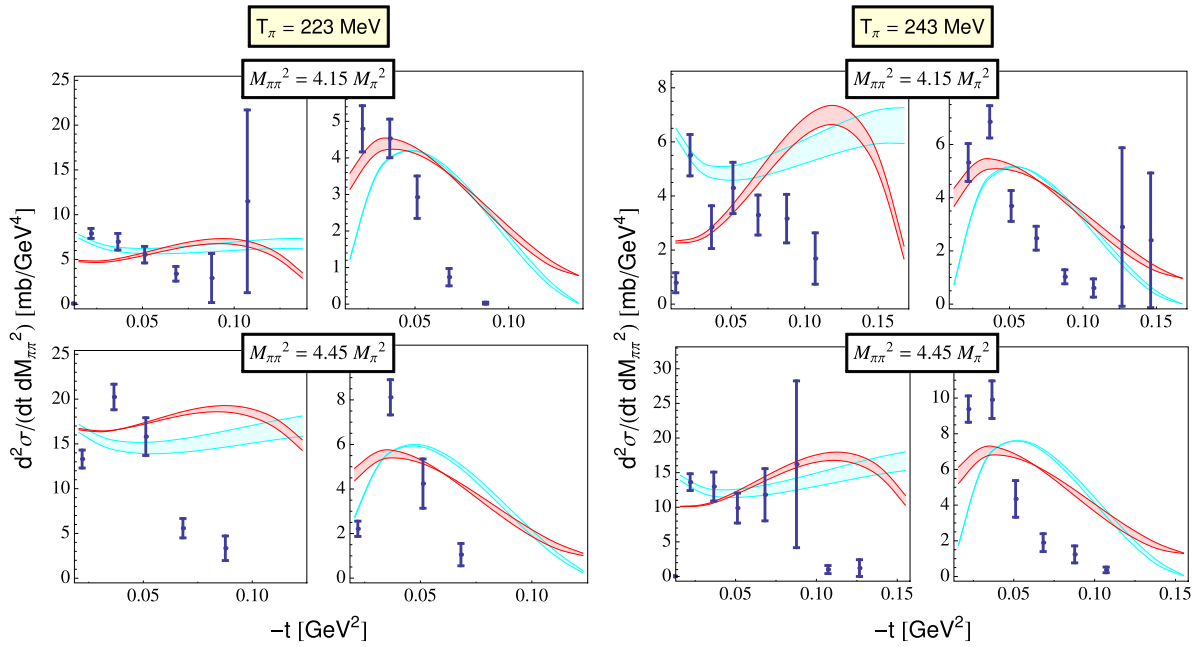

FIG. 12. (Color online) Comparison of NLO relativistic Δ-full and Δ-less χPT predictions for the double-differential cross sections with respect to $M^2_{\pi\pi}$ and t between the two channels $\pi^- p \to \pi^+\pi^- n$ (left) and $\pi^+ p \to \pi^+\pi^+ n$ (right) for two different incoming pion energies; see Eq. (45). For remaining notation see the caption to Fig. 9.

should not come as a surprise given that the predicted total cross section significantly overestimates the experimental data in both the Δ-less and the Δ-full formulations. We also looked at the double-differential cross section $d^2\sigma/(dt dM_{\pi\pi})$ in the same two channels and found large deviations between the theory and the data (see Fig. 12). The large discrepancies between the theory and the experimental data in the $\pi^+\pi^-$ channel, where the single-differential and total cross sections are well reproduced, appear to be somewhat surprising.

Finally, our results for the single-differential cross sections with respect to $\cos\theta$ at the two lowest energies in the $\pi^- p \to \pi^+\pi^- n$ and $\pi^+ p \to \pi^+\pi^+ n$ channels are shown in Fig. 13. Our predictions have the same magnitude as the experimental data but show a different shape. As might be expected from the results for the total cross section, the deviations are most pronounced in the $\pi^+\pi^+$ channel. Note, further, that the effect of the explicit treatment of the Δ isobar is fairly minor for these particular observables.

It is instructive to compare our results with the earlier calculations within the HB [34] and relativistic [35] frameworks. For the total cross sections, our HB results at LO and NLO are very close to the corresponding ones in Ref. [34] and feature similar underprediction of the data for the $\pi^- p$ case. The Q^3 results in that work show a significant improvement, which we now interpret as resulting mainly from taking into account $1/m_N$ corrections. Also, for the double-differential cross sections $d^2\sigma/d\Omega_2 dT_2$, our predictions at $\sqrt{s} = 1242$ MeV at LO and NLO and $\sqrt{s} = 1262$ MeV at LO are close to the ones in Ref. [34]. Our NLO results at the higher energy appear, however, to be significantly closer to the data than those in that work, which probably can be traced back to the different choice of c_i's. While not explicitly shown, we observe that our HB results for other observables are similar to those in [34]. Finally, the order-Q^2 relativistic χPT calculation in Ref. [35] also provides a very useful benchmark for our analysis. We have verified that our results agree with those for

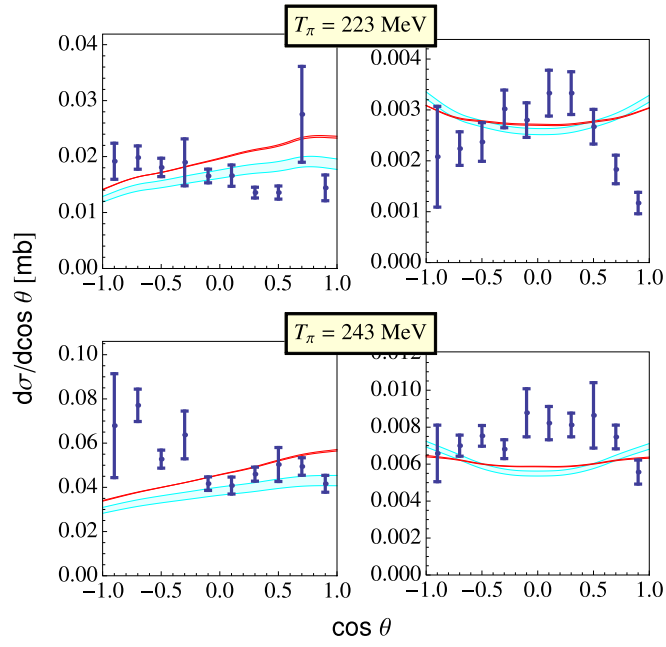

FIG. 13. (Color online) Comparison of NLO relativistic Δ-full and Δ-less χPT predictions for the single-differential cross sections with respect to $\cos\theta$ between the two channels $\pi^- p \to \pi^+\pi^- n$ (left) and $\pi^+ p \to \pi^+\pi^+ n$ (right) for two different incoming pion energies; see Eq. (45). For remaining notation see the caption to Fig. 9.

all observables shown in that work. Finally, we compare with the results in Ref. [26]. Their LO calculation with explicit Δ's and the Roper resonance describes the total cross-section data somewhat better than our LO Δ-full approach, however, it is of a quality similar to that of our NLO Δ-full calculation. It is conceivable that this difference is mostly due to the explicit inclusion of the Roper resonance in Ref. [26]. Note, however, that there is no power counting underlying this calculation, as it only uses the leading dimension 1 derivative pion-baryon couplings.

VIII. SUMMARY AND OUTLOOK

In this paper we have analyzed single-pion production off nucleons at tree level up to NLO using the HB and manifestly covariant formulations of χPT with and without inclusion of explicit Δ isobar degrees of freedom. The main results of our study can be summarized as follows:

(i) We worked out the leading and subleading contributions of the Δ isobar to the invariant amplitudes in the reaction $\pi N \to \pi\pi N$ using both the HB and manifestly covariant formulations of χPT.

(ii) In order to determine the LEC b_i entering the subleading pion-nucleon-Δ Lagrangian, several global fits to the available low-energy data for the total cross sections in the five channels $\pi^- p \to \pi^0\pi^0 n$, $\pi^- p \to \pi^+\pi^- n$, $\pi^+ p \to \pi^+\pi^+ n$, $\pi^+ p \to \pi^+\pi^0 p$, and $\pi^- p \to \pi^0\pi^- p$ have been performed. For the LEC c_i's, which parametrize subleading pion-nucleon interactions, we adopted the values extracted from pion-nucleon scattering. Using the large-N_c predictions for the LECs h_A and g_1 entering the LO Lagrangians $\mathcal{L}^{(1)}_{\pi N\Delta}$ and $\mathcal{L}^{(1)}_{\pi N\Delta}$ and restricting the energy in the fit by $T_\pi = 250$ MeV, the extracted values for the linear combinations $b_4 + b_5$ and $b_3 + b_6$ are found to be of a natural size when using the covariant approach. We observe strong anticorrelations between the LECs b_4 and b_5 as well as b_3 and b_6, which prevent a reliable determination of the linear combinations $b_4 - b_5$ and $b_3 - b_6$. The anticorrelations are found to be much less pronounced if the energy range in the fit is increased up to $T_\pi = 400$ MeV. The resulting values of all LEC b_i's are then found to be of a reasonably natural size. This is in contrast with the fits carried out in the HB approach, where an unnaturally large value for $b_4 + b_5$ is found. Note that in this formulation the amplitude does not depend on the LECs $b_{3,6}$, and the LECs $b_{4,5}$ are also found to be strongly anticorrelated.

(iii) We explored the sensitivity of the total cross section to the LO $\pi\Delta\Delta$ coupling g_1, which is difficult to access in other processes such as, e.g., pion-nucleon scattering, by performing unconstrained fits to the total cross-section data. The resulting values $g_1 = 1.36 \pm 0.73$ and $g_1 = 1.68 \pm 1.38$ in the HB and relativistic formulations, respectively, are (in the HB approach, only barely) consistent with the the large-N_c prediction for this LEC, namely, $g_1 = 2.27$. Extending the fit to 400 MeV within the relativistic formulation leads to a somewhat smaller value of $g_1 = 1.41 \pm 0.22$.

(iv) We found that the covariant framework allows for a clearly superior description of the experimental data at NLO compared to the HB formulation at the same order. Further, as expected, the explicit treatment of the Δ isobar leads to a better description of the data compared to the standard Δ-less formulation, most notably of the $\pi^- p \to \pi^0\pi^0 n$ and $\pi^- p \to \pi^+\pi^- n$ total cross sections at higher energy as well as of the single-differential cross sections with respect to $M_{\pi\pi}$ and t in the $\pi^- p \to \pi^+\pi^- n$ channel. Still, certain single- and double-differential cross sections could not be properly described at this order in the chiral expansion. Finally, we found that there is fairly minor dependence of the extracted LECs and predictions for various observables on the variation in the LEC c_i's used as input in our calculation.

In the future, this work has to be extended in several directions. First, one has to go to the next higher order in the chiral expansion and include pion loop contributions within the covariant framework. This will allow one not only to test the convergence of the chiral expansion, but also possibly to constrain the LEC d_{16}, which governs the quark mass dependence of the nucleon axial vector coupling constant. In addition, it would be very interesting to carry out a simultaneous analysis of the reactions $\pi N \to \pi N$ and $\pi N \to \pi\pi N$. We expect that such a study will result in a more precise determination of the LEC c_i's as compared to elastic pion-nucleon scattering. These LECs govern, in particular, the longest-range three-nucleon force and thus play a prominent role in ongoing studies of few- and many-nucleon systems. It is also conceivable that such a combined analysis will allow for a better determination of the LO pion-Δ coupling constant g_1. As a further step, the explicit inclusion of the Roper resonance might also be considered. Work along these lines is in progress.

ACKNOWLEDGMENTS

We would like to thank Igor Strakovsky for useful comments on the manuscript. This work was supported by the DFG (SFB/TR 16; "Subnuclear Structure of Matter"), the European Community-Research Infrastructure Integrating Activity "Study of Strongly Interacting Matter" (acronym HadronPhysics3; Grant Agreement No. 283286) under the Seventh Framework Programme of the EU, and ERC project 259218 NUCLEAREFT.

APPENDIX: KINEMATICS AND WEIGHT FUNCTIONS

The weight functions y_{ij} appearing in Eq. (27) are defined as

$$y_{11} = -m_N^2 + M_\pi^2 - s + s_1 + s_2 - t_1 - t_2,$$
$$y_{12} = -m_N\left(2m_N^2 + 2s - 2s_1 - 2s_2 + t_1 + t_2\right),$$
$$y_{13} = m_N(-t_1 + t_2),$$

$$
\begin{aligned}
y_{14} &= s(s_1 - s_2) + s_2(s_2 - t_1) + M_\pi^2(t_1 - t_2) \\
&\quad + m_N^2(s_1 - s_2 + t_1 - t_2) + s_1(-s_1 + t_2), \\
y_{22} &= -3m_N^4 + 2M_\pi^4 - M_\pi^2(3s + s_1 + s_2) + s(s + t_1 + t_2) \\
&\quad - m_N^2\big(3M_\pi^2 + 6s - 4s_1 - 4s_2 + t_1 + t_2\big), \\
y_{23} &= ss_1 - ss_2 + s_1t_1 - s_2t_2 + m_N^2(-s_1 + s_2 - t_1 + t_2) \\
&\quad + M_\pi^2(-2s_1 + 2s_2 - t_1 + t_2), \\
y_{24} &= m_N\big(m_N^2 + 2M_\pi^2 + s - s_1 - s_2\big)(2s_1 - 2s_2 + t_1 - t_2), \\
y_{33} &= 3m_N^4 - 2M_\pi^4 - (s - 2s_1)(s - 2s_2 + t_1) - (s - 2s_2)t_2 \\
&\quad - m_N^2\big(5M_\pi^2 - 2s + 2s_1 + 2s_2 + t_1 + t_2\big) \\
&\quad + M_\pi^2(3s - 3s_1 - 3s_2 + 2(t_1 + t_2)), \\
y_{34} &= -m_N\big(m_N^2 - 2M_\pi^2 + s - s_1 - s_2\big) \\
&\quad \times \big(2m_N^2 + 4M_\pi^2 - 2s - t_1 - t_2\big), \\
y_{44} &= \big(m_N^2 + s - s_1 - s_2\big)\big((s_1 - s_2)(-s_1 + s_2 - t_1 + t_2) \\
&\quad + \big(-m_N^2 + s\big)\big(-m_N^2 + s + t_1 + t_2\big)\big) \\
&\quad + M_\pi^2\big(-5s^2 + 4M_\pi^2\big(-M_\pi^2 + 2s\big) - s_1^2 + 6s_1s_2 - s_2^2 \\
&\quad + 2(s_1 - s_2)(-t_1 + t_2) \\
&\quad + m_N^2\big(3m_N^2 - 8M_\pi^2 + 6(s - s_1 - s_2) + 2(t_1 + t_2)\big) \\
&\quad + 2s(s_1 + s_2 - t_1 - t_2)\big),
\end{aligned}
\tag{A1}
$$

where $y_{ij} = y_{ji}$ and the products of the four vectors are expressed in terms of the Mandelstam variables via

$$
\begin{aligned}
2p \cdot q_1 &= s - m_N^2 - M_\pi^2, \\
2p \cdot q_2 &= s - s_2 + t_1 - M_\pi^2, \\
2p \cdot q_3 &= s - s_1 + t_2 - M_\pi^2, \\
2p \cdot p' &= s_1 + s_2 - s - t_1 - t_2 + m_N^2 + M_\pi^2, \\
2q_1 \cdot q_2 &= 2M_\pi^2 - t_1, \\
2q_1 \cdot q_3 &= 2M_\pi^2 - t_2, \\
2q_1 \cdot p' &= s + t_1 + t_2 - m_N^2 - 3M_\pi^2, \\
2q_2 \cdot q_3 &= s - s_1 - s_2 + m_N^2, \\
2q_2 \cdot p' &= s_1 - m_N^2 - M_\pi^2, \\
2q_3 \cdot p' &= s_2 - m_N^2 - M_\pi^2.
\end{aligned}
\tag{A2}
$$

[1] S. Weinberg, Physica A **96**, 327 (1979).
[2] J. Gasser and H. Leutwyler, Ann. Phys. **158**, 142 (1984).
[3] J. Gasser and H. Leutwyler, Nucl. Phys. B **250**, 465 (1985).
[4] J. Gasser, M. E. Sainio, and A. Svarc, Nucl. Phys. B **307**, 779 (1988).
[5] V. Bernard, N. Kaiser, and U.-G. Meißner, Int. J. Mod. Phys. E **4**, 193 (1995).
[6] V. Bernard and U.-G. Meißner, Annu. Rev. Nucl. Part. Sci. **57**, 33 (2007).
[7] V. Bernard, Prog. Part. Nucl. Phys. **60**, 82 (2008).
[8] E. E. Jenkins and A. V. Manohar, Phys. Lett. B **255**, 558 (1991).
[9] V. Bernard, N. Kaiser, J. Kambor, and U.-G. Meißner, Nucl. Phys. B **388**, 315 (1992).
[10] V. Bernard, N. Kaiser, and U.-G. Meißner, Nucl. Phys. A **611**, 429 (1996).
[11] T. Becher and H. Leutwyler, Eur. Phys. J. C **9**, 643 (1999).
[12] J. Gegelia and G. Japaridze, Phys. Rev. D **60**, 114038 (1999).
[13] T. Fuchs, J. Gegelia, G. Japaridze, and S. Scherer, Phys. Rev. D **68**, 056005 (2003).
[14] E. Epelbaum and J. Gegelia, Phys. Lett. B **716**, 338 (2012).
[15] E. E. Jenkins and A. V. Manohar, Phys. Lett. B **259**, 353 (1991).
[16] T. R. Hemmert, B. R. Holstein, and J. Kambor, J. Phys. G **24**, 1831 (1998).
[17] N. Fettes and U.-G. Meißner, Nucl. Phys. A **679**, 629 (2001).
[18] V. Lensky, J. A. McGovern, D. R. Phillips, and V. Pascalutsa, Phys. Rev. C **86**, 048201 (2012).
[19] N. Kaiser, S. Gerstendorfer, and W. Weise, Nucl. Phys. A **637**, 395 (1998).
[20] H. Krebs, E. Epelbaum, and U.-G. Meißner, Eur. Phys. J. A **32**, 127 (2007).
[21] E. Epelbaum, H. Krebs, and U.-G. Meißner, Nucl. Phys. A **806**, 65 (2008).
[22] J. Beringer, PiN Newslett. **7**, 33 (1992).
[23] V. Bernard, N. Kaiser, and U.-G. Meißner, Phys. Lett. B **332**, 415 (1994); **338**, 520(E) (1994).
[24] V. Bernard, N. Kaiser, and U.-G. Meißner, Nucl. Phys. B **457**, 147 (1995).
[25] M. G. Olsson, U.-G. Meißner, N. Kaiser, and V. Bernard, PiN Newslett. **10**, 201 (1995).
[26] T. S. Jensen and A. F. Miranda, Phys. Rev. C **55**, 1039 (1997).
[27] E. Epelbaum, U.-G. Meißner, and W. Glöckle, Nucl. Phys. A **714**, 535 (2003)
[28] E. Epelbaum, U.-G. Meißner, and W. Glöckle, arXiv:nucl-th/0208040.
[29] S. R. Beane and M. J. Savage, Nucl. Phys. A **713**, 148 (2003).
[30] S. R. Beane and M. J. Savage, Nucl. Phys. A **717**, 91 (2003).
[31] J. C. Berengut, E. Epelbaum, V. V. Flambaum, C. Hanhart, U.-G. Meißner, J. Nebreda, and J. R. Pelaez, Phys. Rev. D **87**, 085018 (2013).
[32] E. Epelbaum, H. Krebs, T.A. Lahde, D. Lee, and Ulf-G. Meissner, Phys. Rev. Lett. **110**, 112502 (2013).
[33] E. Epelbaum, H. Krebs, T. A. Lähde, D. Lee, and U.-G. Meißner, Eur. Phys. J. A **49**, 82 (2013).
[34] N. Fettes, V. Bernard, and U.-G. Meißner, Nucl. Phys. A **669**, 269 (2000).
[35] V. Bernard, N. Kaiser, and U.-G. Meißner, Nucl. Phys. A **619**, 261 (1997).
[36] N. Mobed, J. Zhang, and D. Singh, Phys. Rev. C **72**, 045204 (2005).
[37] V. Pascalutsa and D. R. Phillips, Phys. Rev. C **67**, 055202 (2003).
[38] N. Fettes, U.-G. Meißner, M. Mojžiš, and S. Steininger, Ann. Phys. **283**, 273 (2000); **288**, 249 (2001).
[39] H.-B. Tang and P. J. Ellis, Phys. Lett. B **387**, 9 (1996).
[40] V. Pascalutsa, Phys. Lett. B **503**, 85 (2001).

[41] H. Krebs, E. Epelbaum, and U.-G. Meißner, Phys. Lett. B **683**, 222 (2010).
[42] H. Krebs, A. Gasparyan, and E. Epelbaum (unpublished).
[43] B. Long and U. van Kolck, Nucl. Phys. A **840**, 39 (2010).
[44] H. Krebs, A. Gasparyan, and E. Epelbaum, Phys. Rev. C **85**, 054006 (2012).
[45] R. A. Arndt, W. J. Briscoe, I. I. Strakovsky, and R. L. Workman, Phys. Rev. C **74**, 045205 (2006).
[46] R. Koch, Nucl. Phys. A **448**, 707 (1986).
[47] P. Buettiker and U.-G. Meißner, Nucl. Phys. A **668**, 97 (2000).
[48] V. V. Vereshagin, S. G. Sherman, A. N. Manashov, U. Bohnert, M. Dillig, W. Eyrich, O. Jakel, and M. Moosburger, Nucl. Phys. A **592**, 413 (1995).
[49] M. Kermani *et al.* (CHAOS Collaboration), Phys. Rev. C **58**, 3419 (1998).
[50] J. B. Lange, F. Duncan, A. Ambardar, A. Feltham, G. Hofman, R. R. Johnson, G. Jones, M. Pavan *et al.*, Phys. Rev. Lett. **80**, 1597 (1998).
[51] S. Prakhov *et al.* (Crystal Ball Collaboration), Phys. Rev. C **69**, 045202 (2004).
[52] B. Long and V. Lensky, Phys. Rev. C **83**, 045206 (2011).
[53] D. M. Manley, Phys. Rev. D **30**, 536 (1984).
[54] R. Müller, R. Baran, U. Bohnert, P. Helbig, G. Herrmann, A. Hofmann, O. Jaekel, H. Kruger *et al.*, Phys. Rev. C **48**, 981 (1993).